Review

International Journal of Modern Physics E
Vol. 27, No. 7 (2018) 1830004 (57 pages)

DOI: 10.1142/S0218301318300047

World Scientific
www.worldscientific.com

Precision electron beam polarimetry for next generation nuclear physics experiments

Kurt Aulenbacher

Institut für Kernphysik,
Johannes Gutenberg-Universität Mainz,
J.J. Becherweg 45, D-55099 Mainz, Germany

Eugene Chudakov, David Gaskell* and Joseph Grames

Thomas Jefferson National Accelerator Facility,
Newport News, VA 23606, USA
**gaskell@jlab.org*

Kent D. Paschke

University of Virginia, Charlottesville, VA 22904, USA

Received 13 March 2018
Revised 8 June 2018
Accepted 11 June 2018
Published 3 July 2018

Polarized electron beams have played an important role in scattering experiments at moderate to high beam energies. Historically, these experiments have been primarily targeted at studying hadronic structure — from the quark contribution to the spin structure of protons and neutrons, to nucleon elastic form factors, as well as contributions to these elastic form factors from (strange) sea quarks. Other experiments have aimed to place constraints on new physics beyond the Standard Model. For most experiments, knowledge of the magnitude of the electron beam polarization has not been a limiting systematic uncertainty, with only moderately precise beam polarimetry requirements. However, a new generation of experiments will require extremely precise measurements of the beam polarization, significantly better than 1%. This paper will review standard electron beam polarimetry techniques and possible future technologies, with an emphasis on the ever-improving precision that is being driven by the requirements of electron scattering experiments.

Keywords: Electron polarimetry; Mott polarimeter; Møller polarimeter; Compton polarimeter; parity violation.

PACS Number(s): 29.27.Hj, 24.70.+s, 24.80.+y

*Corresponding author.

1. Introduction

The use of spin-polarized electron beams has been an important tool for illuminating the fundamental nature of electron interactions and for the study of the atomic nucleus. In any such measurement, the precision of the measurement of a spin-dependent scattering rate cannot exceed the precision of knowledge on the electron beam polarization. Electron beam polarimetry is required for a broad program of study, with technological improvement that has generally kept this technology from becoming a limiting factor in the experimental precision. Future measurements, however, have been proposed which will push the boundaries of polarimetry precision. The purpose of this paper is to review the state-of-the-art in electron beam polarimetry at the moderate beam energies most relevant for the near future programs at fixed-target electron beam facilities.

The earliest productive studies using a polarized electron beam took place at the Stanford Linear Accelerator in the early 1970s, with a polarized source based on photoionization from a polarized atomic beam providing tens of nanoamps with $\sim$80% polarization. This beam was first used for high-energy polarized electron scattering with a magnetized ferromagnetic foil target,[1] demonstrating the utility of this target for electron beam polarimetry. This was followed by measurements using a polarized proton solid target to measure the proton elastic form-factors[2] and pursue the first study of spin structure functions[3] in deep inelastic scattering, topics which have remained prominent in electromagnetic spin physics. A broad range of elastic form-factor studies of the proton and neutron[4] has been performed using polarized solid and gas targets, and recoil polarimetry. A highlight of these form-factor studies is a measurement of the ratio of proton form-factors G_E^p/G_M^p using recoil proton polarimetry[5] which sharply disagreed with results from unpolarized cross-section measurements at 4-momentum transfers above $Q^2 \sim 1\,\mathrm{GeV}^2$, leading to a re-evaluation of conclusions from decades of elastic form-factor studies. Investigations of the proton and neutron spin structure were spurred on by results from the European Muon Collaboration (EMC) that showed unexpectedly low values for the net spin polarization of the quarks in the nucleon. Polarized deep-inelastic scattering measurements at the SLAC, HERMES at the Deutsches Elektronen-Synchrotron (DESY), and the Thomas Jefferson National Accelerator Facility (JLab) have continued to refine the picture of nucleonic spin.[6]

In addition to the electromagnetic interaction, the electron also interacts through the weak force. Although the weak interaction amplitude is small at moderate energies, it can be distinguished from the electromagnetic interaction by taking advantage of the fact that the weak interaction violates the parity symmetry. The first measurement of parity violation in electron scattering (PVeS) was made at SLAC in 1978 in order to help to establish the Weinberg–Salam–Glashow model of electroweak unification.[7] This experiment utilized a polarized source based on photoemission from a semiconducting GaAs cathode, which produced several microamps of beam current with a polarization of around 40%. This source was

more robust than the source based on an atomic beam, and the polarization could be rapidly reversed, without otherwise altering the quality of the electron beam, by reversing the polarization of the light incident on the photocathode. This nondisruptive, rapid reversal allows for greater precision in the measurement of a polarization-dependent asymmetry. A broad range of PVeS measurements has since determined the weak neutral current form-factors of the proton,[8] benchmarked the neutron distribution in heavy, neutron-rich nuclei,[9] or searched for contributions to PVeS beyond the Standard Model of electroweak interactions.[10–12]

These weak interaction studies have generally driven improvements in the precision of electron beam polarimetry. For accelerated electron beams, the transverse spin polarization is suppressed by $1/\gamma$, so in most cases only observables depending on the longitudinal electron polarization P_z are of interest. For this reason, electromagnetic studies, which must respect the parity symmetry, measure observables that combine the electron polarization with target or recoil polarization, which is typically determined with less precision than the electron polarization. The single-spin analyzing power measured in PVeS depends only on the beam electron longitudinal polarization, so knowledge of this polarization can become the dominant systematic error.

Various examples of measurements relying on electron beam polarimetry are listed in Table 1 to highlight the range of conditions and applications for experiments utilizing polarized electron beams. Examples in which the parity-conserving double-spin asymmetries are measured are the JLab proton form-factor measurements[5] using Mott and Møoller beam polarimetry with recoil polarimetry of the scattered proton, the SLAC-E154 measurement[13] of neutron spin structure using Møoller beam polarimetry with a ^{3}He polarized target, and the HERMES spin structure program[14] using a polarized positron beam in a storage ring, measured by Compton polarimetry and scattered from polarized internal gas targets. The increasing precision of parity-violation measurements, in which beam polarimetry can be the largest nonstatistical uncertainty, is evident in the progression from the pioneering SLAC-E122 experiment[7] utilizing Møoller polarimetry at high energy, the Bates SAMPLE experiment[15] and MAMI PV-A4[16] measurements at low energy

Table 1. Examples of measurements relying on electron beam polarimetry.

Experiment	Beam energy	Polarization	Polarimetry precision
JLab GEp/GMp (1999)[5]	1–4 GeV	60%	3%
SLAC E154 DIS $g1n$ (1997)[13]	48 GeV	82%	2.4%
HERMES $g1n$ DIS (2007)[14]	30 GeV	55%	2.9%
SLAC 122 PV-DIS (1978)[7]	16–22 GeV	37%	6%
Bates SAMPLE (2000)[15]	0.2 GeV	39%	4%
MAMI PV-A4 (2004)[16]	0.85 GeV	80%	2.1%
JLab Qweak (2017)[11]	1.2 GeV	88%	0.62%
SLD A_{LR} (2000)[17]	46.5 GeV	75%	0.5%

using Møoller polarimetry, and the recent Qweak experiment[11] at JLab utilizing Møoller and Compton polarimetry. In addition to those measurements at fixed target facilities, the parity-violating A_{LR} measurement from electron–positron collisions with SLD at SLAC, which used Compton polarimetry near the interaction point, is listed[17] for comparison.

These measurements have made use of three techniques in order to determine the absolute longitudinal beam polarization. The techniques are based on scattering the polarized electron beam from unpolarized nuclei (Mott scattering), polarized atomic electrons (Møller scattering), or polarized photons (Compton scattering). Because they are effective at high energies, the Møller and Compton polarimeters are often built near the experimental target, to minimize corrections due to beam loss, depolarization, or spin precession during beam transport.

Mott polarimeters are effective only at low beam energies (below 10's of MeV), and are often used near the beam source, before acceleration to highest energy. Mott scattering is only sensitive to transverse beam polarization, so a complete polarization measurement requires spin manipulation to vary the polarization orientation of the incident beam. For high-energy experiments, the results of a Mott measurement must then be extrapolated, through calculation or measurement of the spin precession during beam transport, to the experimental target. While the polarization on target is instead most often measured using high-energy polarimeters, a Mott polarimeter is an important tool for optimizing the polarized source performance and setting the initial polarization orientation.

For each polarimeter, the scattering cross-section depends on the polarization of the electron beam, and the polarization is determined using the cross-section asymmetry under reversal of the beam polarization. Taking as an example the Compton (electron–photon) scattering process, the cross-section depends on the longitudinal polarizations of the beam P_b and photon P_γ, as $\sigma = \sigma_0(1 + P_b P_\gamma A_{ZZ})$. Here, σ_0 is the unpolarized cross-section and A_{ZZ} is referred to as the analyzing power. For a fixed photon polarization, the beam polarization is deduced from an asymmetry measurement which compares cross-sections with right- and left-handed beam polarization:

$$A_{\mathrm{RL}} = \frac{\sigma_R - \sigma_L}{\sigma_R + \sigma_L}. \tag{1}$$

The electron beam produced from the photoemission source reverses polarization with minimal difference in polarization magnitude: $P_b = P_b^R = -P_b^L$. In this case, $A_{\mathrm{RL}} = P_b P_\gamma A_{ZZ}$. With knowledge of the photon polarization and the analyzing power, the beam polarization P_b can be deduced. If the polarization magnitude is different between the polarization states, $P_b^{R(L)} = \pm P_{b0} + \delta P$, then the measured asymmetry is no longer proportional to the beam asymmetry and the analyzing power. At leading order, a correction is required:

$$A_{\mathrm{RL}} = P_{b0} P_\gamma A_{ZZ} - P_{b0} \delta P (P_\gamma A_{ZZ})^2.$$

This correction is thought to be vanishingly small for published measurements. For example, the recent Qweak experiment[11] at 1 GeV beam energy saw a peak analyzing power of $A_{ZZ} \sim 4\%$, so even δP as large as 1% would imply a correction of only 0.04%. For measurements at higher energy, where the analyzing power may be 30% or higher, $\delta P \sim 1\%$ would imply an effect at the level of 0.3%. For a photoemission polarized source, it is expected that illumination by equal-but-opposite laser polarization states will give symmetric polarization to the emerging electron beam. That is, for opposite laser polarization state, the excitation of the corresponding electron polarization state in the photocathode and the subsequent partial depolarization of the electron as it exits the material are thought to be the same. In principle, a significant difference δP could also arise from a significant difference in the polarization of the incident laser light. This would require a gross error in configuration in the laser optics, which would likely be noticed and corrected. So, while the expected effects are small, the stringent requirements of future high precision experiments suggest that direct verification would be prudent.

A series of future experiments testing the boundaries of the Standard Model will push the precision requirements for electron beam polarimetry to new limits. The P2 collaboration[18] at Mainz will use the new MESA facility with an extracted beam to measure the proton weak charge with a precision of 1.5%, at a very low beam energy of about 150 MeV. The MOLLER experiment[19] at JLab will measure electron–electron scattering to 2.4% relative error, while the JLab SOLID collaboration[20] proposes a measurement of PVeS in the deep-inelastic regime with a total precision of 0.5%. Reaching these precision goals at the very low energy of P2 or the very high precision of SOLID motivates continued improvement in polarization techniques.

Beyond that program of fixed-target measurements, a future polarimetry challenge will also be found at the proposed electron-ion collider,[21] which will use polarized ion and electron beams. The planned electromagnetic studies require electron polarimetry at the level of 1–2%, but a program of PVeS study for partonic spin-structure functions has been proposed which will require a 0.5% precision on the electron polarization in the challenging collider environment.

2. Mott Polarimetry

Mott polarimeters use the single-spin asymmetry in the scattering of (transversely) polarized electrons from the nucleus of a large Z target. The analyzing power for this process is large at MeV-scale energies, making it an ideal tool for polarization measurements near the polarized electron source. Since the target is not polarized, construction and deployment of a Mott polarimeter is somewhat simpler compared to Møller and Compton polarimeters (discussed later).

In the late 1920s, Mott considered the spin-dependent implications of an electron scattering from the bare nuclear charge of an atom.[22] In the classical interpretation, large angle scattering corresponds to a small impact parameter, where the scattered electron experiences a significant magnetic field in its rest frame from motion within

the electric field of the nucleus. The resulting spin-orbit interaction potential leads to a term in the cross-section which then depends upon the component of the spin normal to the scattering plane.

So-called Mott polarimeters are constructed to exploit this principle. A pair of detectors are arranged opposing one another to measure the counting rates of electrons elastically scattered e.g., to the left and right (or up and down) from a target foil. The counting rate asymmetry between a pair of detectors (e.g., between left and right) is then proportional to the component of the beam polarization normal to the scattering plane defined by those two detectors. The counting rate asymmetry is also proportional to the analyzing power, known as the Sherman function. The Sherman function is a theoretically calculated value for single-atom scattering and depends upon the electron kinetic energy, the atomic number of the target nucleus and the scattering angle from the atom. In real targets, some electrons elastically scatter more than once before being detected. Consequently, a reduced analyzing power known as the effective Sherman function must be determined, typically by experimental extrapolation of thick targets to the single-atom value. The precise shape of the extrapolation is explored both empirically and by simulations. Electrons that are detected but have suffered inelastic collision or do not originate from the target foil dilute the effective analyzing power. To demonstrate precise absolute measurement of the beam polarization such background events must be carefully understood and, if possible, suppressed.

At low electron beam energies, Mott scattering is a technically appealing method due to its large analyzing power and cross-section. For this reason, Mott polarimeters are often associated with polarized electron sources. Consequently, many useful references exist in the case when the electron beam energy is that of a DC high voltage electron gun[23] (>50 kV). Another variant, found in the laboratory environment to study polarized sources, is the retarding potential Mott polarimeter[24–26] wherein a small accelerating voltage (<50 kV) is applied only for the purpose of Mott scattering. Two useful review papers on low energy Mott scattering may be found in Refs. 27 and 28.

Owing to the high scattering probability, Mott polarimeters at this low energy are characteristically limited to operate at very low beam intensity (<10 nA) and/or with very thin target foils (<100 nm), which are fragile, and for the thinnest type require a low-Z backing material. In either case, the high scattering probability tends to dilute the effective analyzing power through multiple scattering and leads to increased backgrounds. Both of these factors lead to increased uncertainty in the effective Sherman function, and consequently limit the ultimate accuracy of the electron polarization to the percent level.

A modern variation discussed below is the MeV energy Mott polarimeter. The primary advantage when operating at higher energy is that the cross-section becomes meaningfully reduced, with counting rates typically <1 kHz/μA/μm. Practically, this allows one to operate with higher beam current (>1 μA) and free-standing and more manageable target foils (>100 nm). The higher energy is

typically achieved in an electron accelerator with RF beam structure, thus the usual intensity or beam position diagnostics of accelerated beams may be used to better understand and control systematics. At larger energy (smaller impact parameter) the single-atom Sherman function is greater and the dilution, due to either double-elastic scattering or backgrounds not associated with the target foil, is smaller. All of these factors lead to a smaller uncertainty in the analyzing power, but also an improved figure-of-merit (FOM), IS^2. At even higher energy (>10's MeV) Mott polarimeters become impractical, as the cross-section drops rapidly and the scattering angle of the maximum Sherman function approaches the incident beam direction. Further, at these higher energies finite nuclear size effects lead to corrections resulting in uncertainties in the analyzing power larger than 1%, make this a challenging option for precision polarimetry.

Overall, Mott polarimeters offer a simple footprint, operate with unpolarized targets and have a high counting rate for precise rapid measurements (<1% in 5 min). However, they are invasive to normal beam operation, require a set of targets to extrapolate to the single-atom Sherman function, and often require spin rotators to align the beam polarization transversely. Also, Mott polarimeters are typically located far from the main nuclear physics experiment.

2.1. *Cross-section and Sherman function*

The Mott differential cross-section for an electron scattering at an angle θ from a target atom of nuclear charge (Z) may be calculated using the Dirac equation to yield

$$\sigma(\theta, \phi) = I(\theta)[1 + S(\theta)\mathbf{P} \cdot \hat{n}], \tag{2}$$

where $I(\theta)$ is the unpolarized cross-section

$$I(\theta) = \left(\frac{Ze^2}{2mc^2}\right)^2 \cdot \frac{(1-\beta^2)\left(1-\beta^2 \sin^2\left(\frac{\theta}{2}\right)\right)}{\beta^4 \sin^4\left(\frac{\theta}{2}\right)}, \tag{3}$$

and $S(\theta)$ is the single-atom analyzing power (Sherman function), $\mathbf{P}$ is the incident electron polarization, $\hat{n} = \frac{\mathbf{k}\times\mathbf{k}'}{|\mathbf{k}\times\mathbf{k}'|}$ is the unit vector normal to the scattering plane where $\hbar\mathbf{k}$ ($\hbar\mathbf{k}'$) is the incoming (outgoing) electron momentum. An important feature of Eq. (2) is that only the component of the beam polarization normal to the scattering plane contributes to the scattering asymmetry.

The Sherman function dependence on scattering angle from a gold atom ($Z = 79$) for electron beam energies commonly found at polarized electron sources or injectors is shown in Fig. 1. A striking feature is that over a broad range of beam energies the analyzing power remains large, e.g., 40–50% between 100 keV and 5 MeV.

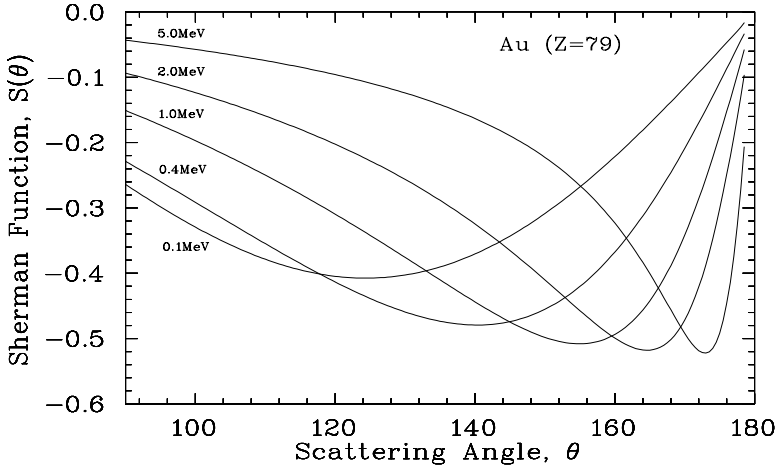

Fig. 1. The Mott scattering analyzing power for gold as a function of scattering angle and electron energy. Figure reproduced from Ref. 27 with minor modifications.

2.1.1. *Mott asymmetry measurement*

Consider a Mott polarimeter with a pair of detectors arranged above (up) and below (down) a target foil defining the normal ($\hat{n}$) to the vertical scattering plane. An electron beam with fully horizontal polarization $\mathbf{P}$ may be either parallel or anti-parallel to $\hat{n}$. The number of electrons scattered through an angle θ *up* and detected, N_u, is proportional to $1 + \mathrm{PS}(\theta)$. Similarly the number scattered *down* and detected, N_d, is proportional to $1 - \mathrm{PS}(\theta)$. The experimental asymmetry (ϵ) is defined as the difference in the number of electrons scattered up versus down divided by their sum

$$\epsilon = \frac{N_u - N_d}{N_u + N_d} = \mathrm{PS}(\theta). \tag{4}$$

Although Eq. (4) can be used to compute the experimental asymmetry, instrumental errors between the detectors introduce uncertainty in the measured polarization. These errors are introduced by inequalities in the pairs of detectors, or misalignments and inhomogeneities in the beam or target. Consider again the *up* and *down* detectors where the beam is well-aligned and scatters into both detectors at an angle θ. The efficiencies (Q_u, Q_d) and solid angles ($\Delta\Omega_u$ and $\Delta\Omega_d$) of the detectors can be different. For a beam of spin-right (+) electrons the number of scattered elastic electrons detected are then

$$\begin{aligned} N_u^+ &= i^+\rho^+ Q_u \Delta\Omega_u I(\theta)[1 + \mathrm{PS}(\theta)], \\ N_d^+ &= i^+\rho^+ Q_d \Delta\Omega_d I(\theta)[1 - \mathrm{PS}(\theta)], \end{aligned} \tag{5}$$

where i^+ and ρ^+ are the beam current and target density for this spin state. If $Q_u\Delta\Omega_u \neq Q_d\Delta\Omega_d$ an experimental asymmetry due to the detectors exists. This

can be eliminated by reversing the helicity of the electron beam, e.g., at the source or via spin manipulation. Then the spin-left (−) electrons are detected

$$\begin{aligned} N_u^- &= i^- \rho^- Q_u \Delta\Omega_u I(\theta)[1 - \mathrm{PS}(\theta)], \\ N_d^- &= i^- \rho^- Q_d \Delta\Omega_d I(\theta)[1 + \mathrm{PS}(\theta)], \end{aligned} \tag{6}$$

where i^- and ρ^- are the beam current and target density for this spin state. These two equations can be combined to produce

$$\begin{aligned} \sqrt{N_u^+ N_d^-} = N^+ &= \sqrt{i^+ i^- \rho^+ \rho^- Q_u Q_d \Delta\Omega_u \Delta\Omega_d} I(\theta)(1 + \mathrm{PS}(\theta)), \\ \sqrt{N_u^- N_d^+} = N^- &= \sqrt{i^+ i^- \rho^+ \rho^- Q_u Q_d \Delta\Omega_u \Delta\Omega_d} I(\theta)(1 - \mathrm{PS}(\theta)). \end{aligned} \tag{7}$$

The experimental asymmetry is then computed by calculating the super-ratio

$$\epsilon = \frac{N^+ - N^-}{N^+ + N^-} = \mathrm{PS}(\theta), \tag{8}$$

which is independent of the beam current and target uniformity between helicity states (assuming no other helicity dependencies), and the detector solid angle and efficiencies. It is straightforward to show that the uncertainty in the determined polarization is $\Delta P = 1/\sqrt{N \cdot S(\theta)^2}$. Extended details and various case examples are thoroughly considered in the text by Kessler.[29]

2.1.2. *Theoretical Sherman function*

Measuring the polarization dependence by exploiting Eq. (2) requires theoretical knowledge of the Sherman function $S(\theta)$. For elastic scattering, $S(\theta)$ is expressed[29] via the direct amplitude, f, and the spin-flip amplitude, g, which depend on the scattering angle θ and beam energy E:

$$S(\theta) = i\frac{fg^* - gf^*}{f^2 + g^2}, \tag{9}$$

where i is the imaginary unit and * is the complex conjugate. For elastic electron scattering in a potential generated by an arbitrary spherically symmetric charge distribution (e.g., a spin zero nucleus with closed shell electronic cloud) the functions $f(\theta, E)$ and $g(\theta, E)$ can be calculated exactly as a function of scattering angle and energy (see formula 1A-109 in Ref. 30). Apart from numerical uncertainties, only the modeling uncertainty of the potential due to unknown details of the nuclear charge distribution and atomic electron distribution generates a systematic error in $S(\theta)$. The level of accuracy in numerically computing $S(\theta)$ has improved since earliest treatments; from that of a point-like nucleus,[31] to the inclusion of finite nuclear size,[32] to the modern treatment that includes the best available nuclear and atomic structure data.[33]

Energies between 2 MeV and 10 MeV can be considered as a region where these uncertainties can be kept under control at a level of 0.5% or better. This is because

the momentum transfer is high with respect to the electron momenta but low enough to be relatively insensitive to the details of nuclear structure. For instance the effect of finite nuclear size on the scattering asymmetry from Pb-208 was measured to be of the order of 20% at 14 MeV and 172°.[34] With a typical uncertainty of 2% for the nuclear radius, the contribution to the uncertainty in the Sherman function is still below 0.5% and becomes even smaller for energies below 10 MeV. The contribution from Coulomb screening, while large at low beam energy,[35] becomes small (<0.3%) in this energy range, except at forward scattering angles where it represents a correction[36] of a few percent. The effects of electron exchange potential and absorptive losses due to quasi-elastic collisions with the atomic electrons are calculable, however, these effects are small (<0.2%)[36] or negligible.

Presently, the leading uncertainties in the Sherman function result from radiative effects. These can be divided into internal effects, which (in leading order in the fine structure constant) are the vacuum polarization and self-energy contributions, and external bremsstrahlung radiation. In the case of internal radiative effects, the contribution due to vacuum polarization e.g., for gold ($Z = 79$) and 5 MeV is <0.5%.[36] The self-energy contribution has not been reliably calculated yet however, there is reason to believe that the vacuum and self-energy corrections are of opposite sign and tend to cancel one another.[37] The effect of bremsstrahlung has been treated in an early paper[38] in which an upper limit of this contribution to the Sherman function was estimated to be 0.8% at 600 keV, however, that calculation has yet to be extended to MeV energy Mott polarimeters, where the higher energy would be expected to increase the contribution but the larger scattering angle would suppress it.

The strongest statement about radiative corrections (both external and internal) comes from experimental evidence. Two experiments, one with an energy variation of 1–3.5 MeV,[39] and another from 2.75 MeV to 8.2 MeV,[40] were performed. In each experiment a polarized electron beam was scattered from a series of targets for the purpose of extrapolation to zero-thickness, but over a range of beam energies. In these experiments the extrapolated values of the Sherman function were consistent at the level of ±0.5% (see Fig. 2) and ±0.4% (see Fig. 3), respectively. Because it is highly unlikely that radiative corrections are independent of energy, these results suggest that their contribution to the Sherman function is considerably smaller than 1%.

In summary, modern calculations include realistic nuclear and atomic potentials allowing one to accurately calculate these contributions to the Sherman function to the tenths of a percent level. The limiting uncertainties arise from radiative corrections. Experimental evidence suggests that radiative effects collectively may be no larger than 0.5% for MeV energy Mott polarimeters, however, this leading uncertainty must continue to motivate the level of theoretical and experimental investigation to reduce the uncertainty presently believed in the range of 0.5–1%.

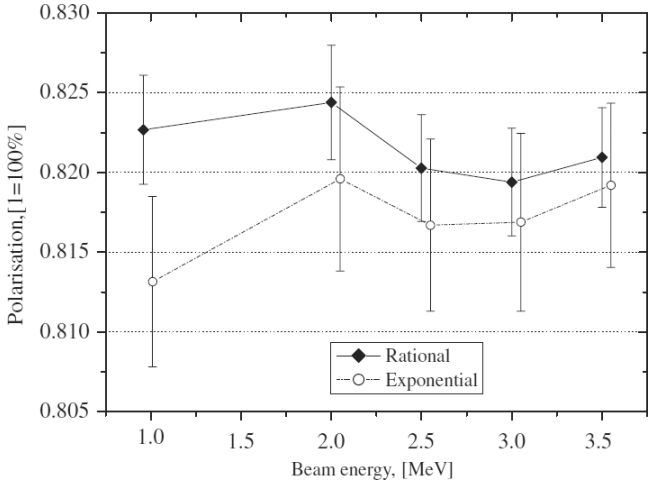

Fig. 2. Extrapolation result for two different fit functions as a function of energy. Figure from Ref. 39. The scattering of extrapolated values in each state is smaller than ±0.5%.

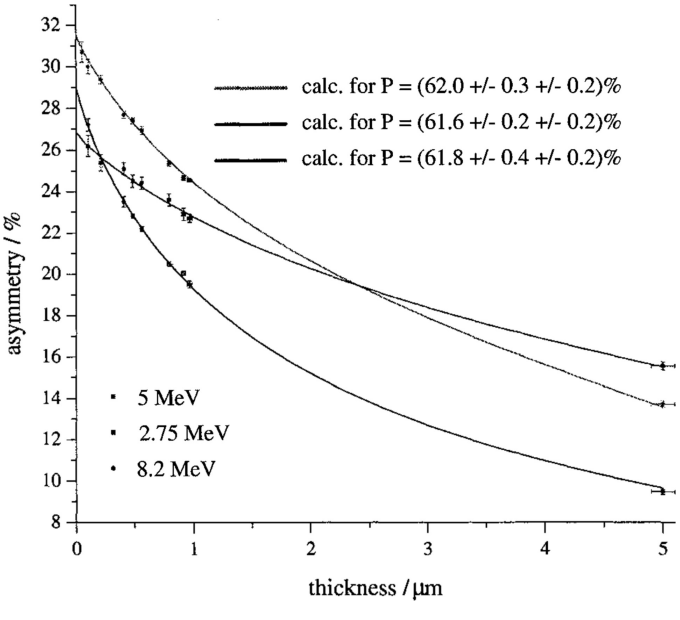

Fig. 3. Foil-thickness extrapolation for 2.75, 5 and 8.2 MeV. Lines symbolize calculation and dots the measurement. Figure from Ref. 40.

2.1.3. *Effective Sherman function*

Because of multiple scattering, the measured Mott asymmetry varies with the thickness of the target. As an example, Fig. 4 demonstrates the asymmetry of a 4.7 MeV transversely polarized electron beam scattering from a series of thin gold target

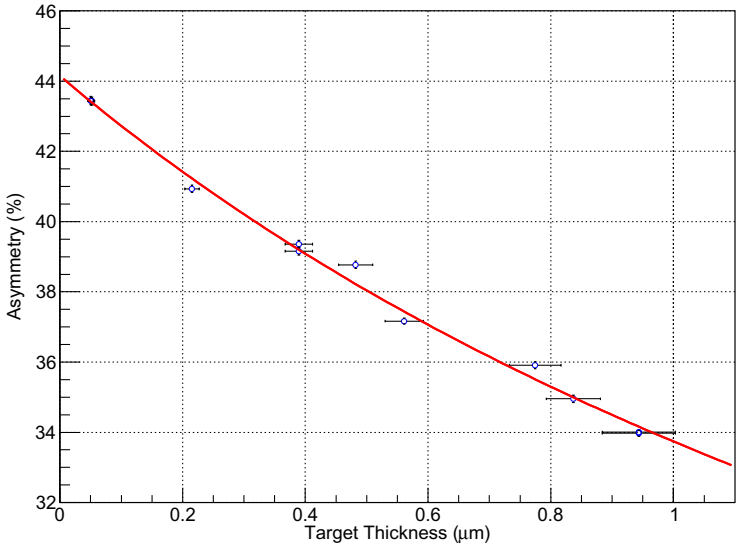

Fig. 4. Target foil extrapolation asymmetries measured using the Continuous Electron Beam Accelerator Facility (CEBAF) Mott polarimeter with a 4.7 MeV polarized electron beam and gold foils of varying thickness.

foils. The decrease in asymmetry with target thickness is due to the combination of plural and multiple scattering,[a] i.e., the electrons arriving at the detector which have undergone multiple/plural elastic scattering in the target foil will carry a lower asymmetry than those which arrive after one scattering event. High energies are favorable since for a given target thickness the relative contribution of multiple/plural scattering is smaller. For example, the reduction of analyzing power from a zero-thickness target to one 100 nm thick is 20% for a 100 keV beam[41] whereas the corresponding reduction at 4.7 MeV is only about 3% (see Fig. 4).

In order to minimize systematic uncertainties, very thin targets are utilized at low energies which themselves introduce new problems, for instance due to inhomogeneous formation of the gold films. In the MeV case the slope is very small which not only allows the use of relatively robust targets but also gives some tolerance against errors in the target thickness.

The reduced analyzing power, or *effective Sherman function*, is determined by measuring the diluted analyzing power for target foils of varying thickness and extrapolating to zero-thickness so that one may normalize to the theoretically determined single-atom Sherman function. Historically, the extrapolation has been

[a]Many small angle scatterings combined with one large angle scattering are called "multiple scattering" and a process containing a few large angle scatterings is called "plural scattering". Note the prominent role of a 90° first scattering in case of perpendicular incidence on the target: For particles scattered in this direction the target is of infinite thickness and a second scattering into the backward direction is probable.

performed by choosing one of a variety of empirical or model driven functional forms which lead to systematic uncertainties at the 1% level, e.g., see Ref. 42. Alternatively, others have approached the extrapolation by means of a Monte Carlo simulation to numerically evaluate and predict the dilution with target thickness, e.g., at 120 keV[42] and at MeV energies.[40,41] New results (in preparation) at Jefferson Lab that test the accuracy of the CEBAF 5 MeV Mott polarimeter by a statistical approach and numerical methods both suggest even further suppression of this uncertainty and improved predictive power. Generally, the systematic uncertainty associated with the effect of multiple/plural scattering is well in hand and expected to be suppressed below 0.5% in the MeV region.

2.2. *MeV Mott polarimeters*

2.2.1. *CEBAF MeV Mott polarimeter*

Figure 5 depicts the Mott polarimeter at the CEBAF at Jefferson Lab. A long vertical ladder supports up to 14 target foils to perform studies of the effective Sherman function using foils with different thicknesses and atomic number. The vacuum is maintained by a 45 L/s DI ion pump and a nonevaporable getter (NEG) pump. An overboard pump with backed butterfly valves is used to protect thin foils from turbulent flow when venting the chamber. An *in situ* polished stainless steel disk collects visible light from a view screen and optical transition radiation (OTR) from a target foil to monitor the beam position during operation. The polarimeter was optimized for 5.0 MeV, but has been studied over the range of 3–8 MeV and with target foils of Au, Ag and Cu.[43]

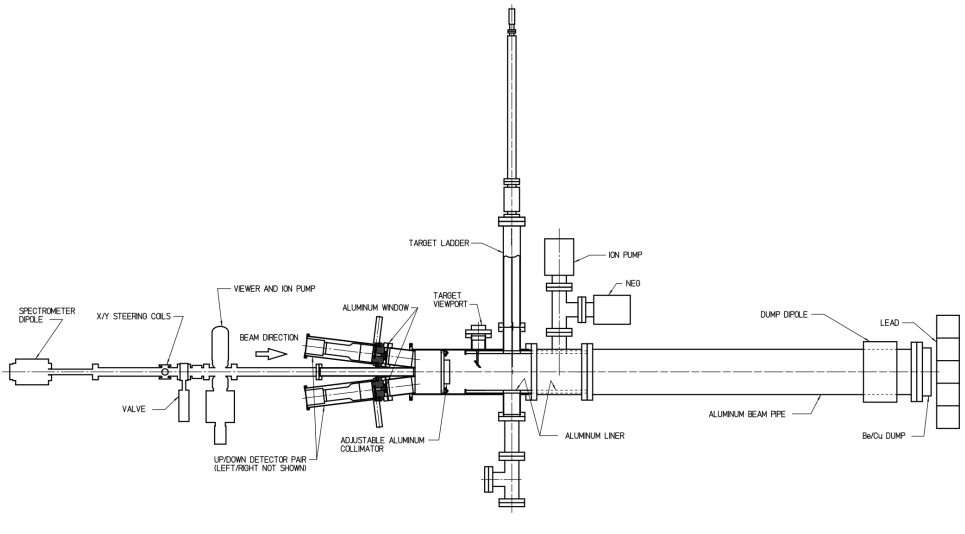

Fig. 5. CEBAF Mott polarimeter beam line indicating beam line components: Scattering Chamber, Extension Spool, Beam Tube/Dump.

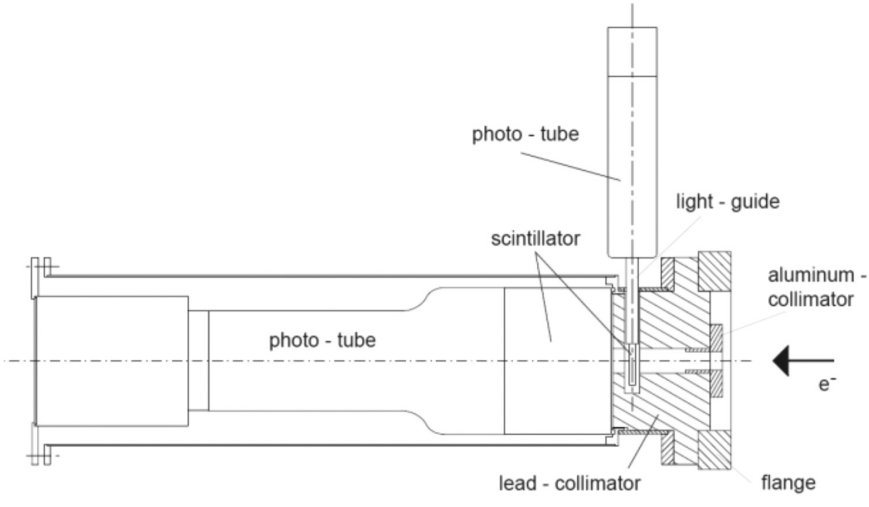

Fig. 6. CEBAF Mott detector assembly.

Four detectors, arranged azimuthally, simultaneously measure both the horizontal and vertical components of the beam polarization. A fixed collimator upstream of the target ladder defines the scattering angle (172.7°) and detector acceptance (0.232 msr). Electrons passing the collimator exit the vacuum chamber through thin 0.05 mm Al windows before reaching the detector package (Fig. 6). Each detector package consists of a thin scintillator and PMT insensitive to photons followed by a thick scintillator and PMT to fully absorb the energy of each incident electron. Each pair of detectors operates in coincidence to veto photons and provide an energy resolution of $<2\%$.

The electron bunch spacing at CEBAF is 2 ns. However, electrons which back-scatter from the beam dump or chamber walls may return to the target foil up to 12 ns later just as new bunches are arriving, representing a possible background. Significant efforts were made to mitigate and isolate events not originating from the target foil. The stainless steel vacuum chamber surfaces and long beam tube extending from the target to the dump are lined with or composed of aluminum. The beam dump itself is faced with a beryllium disk to minimize back-scatter and followed by a thick copper flange which absorbs most of the beam power via ionization losses and radiates remaining power toward an air-side lead wall.

To achieve a high precision assessment of the effective Sherman function, special measurements were performed with sub-harmonic bunch spacing of 16 ns or greater, where all activity from one electron bunch entering the polarimeter is measured before the next bunch arrives. An example spectrum from such a study operating at a repetition frequency of 31.1825 MHz is shown in Fig. 7. This approach allows for a precise measurement of only those events elastically scattering from the target foil, critical for achieving a precise extrapolation to the single-atom Sherman

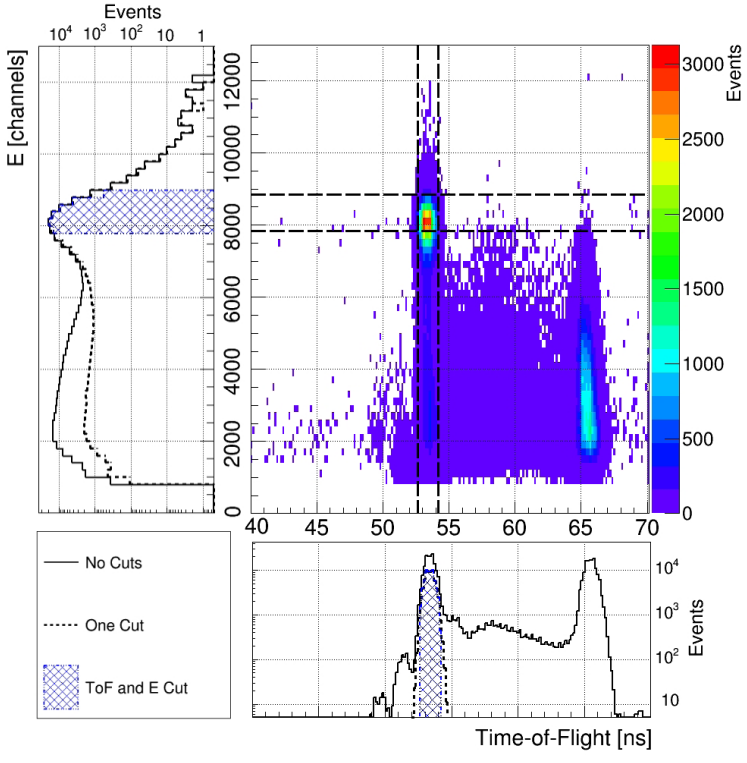

Fig. 7. A typical energy versus timing spectrum when operating the beam at 31.1875 MHz demonstrates separation of events originating from the target foil (54 ns) from those returning from the beam dump originating from an earlier time (66 ns), revealing ∼12 ns round trip time. The projected histograms show events remaining after imposing the parameter cut applied (dashed line) or when both standard cuts are applied (hashed area).

function. Once completed, a correction for operation with the usual 2 ns bunch spacing was determined by repeating the analysis without considering any cut on the bunch timing. This revealed a sub-percent correction required for the thinnest foils where backscattering quasi-elastic events from the dump are detectable, however, the contribution becomes negligible as the target thickness is increased.

2.2.2. *MAINZ MeV Mott polarimeter*

Similar to the approach at JLab, a Mott polarimeter[39] was installed behind the MAMI Injector Linac (ILAC).[44] The device is located in a special beam line into which the polarized beam can be deflected by a magnet located between the injector and the first microtron of MAMI. The output energy of the ILAC can be varied between 1 MeV and 3.5 MeV. The main difference with regard to the approach in the preceding section is the method of background suppression. Figure 8 shows a schematic of the apparatus.

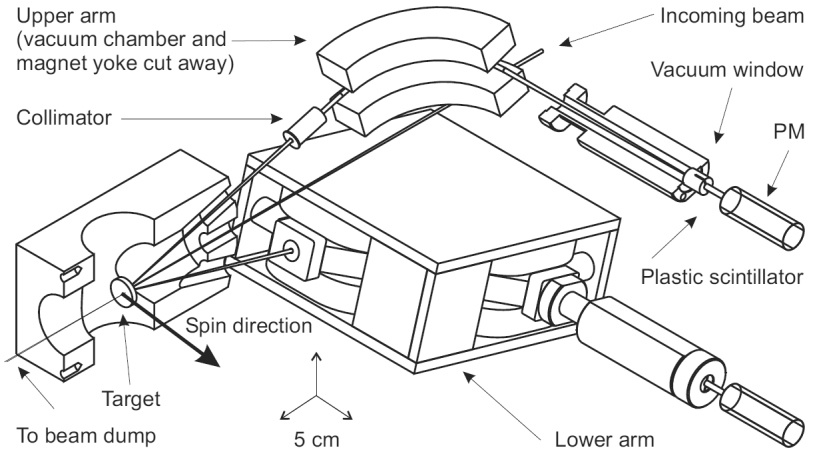

Fig. 8. Schematic view of the Mott polarimeter at MAMI. Figure from Ref. 39.

Electrons are scattered by 164°. At this angle, the Sherman function peaks for an input energy of 2 MeV. Stigmatic imaging of the beam spot at the target onto the detector is achieved by using deflection magnets with inhomogeneous magnetic fields. The corresponding focusing strength allows for a compact set up. The deflection by the magnet removes the detector scintillator from direct line-of-sight to the beam dump and allows good lateral shielding. Multiple targets can be moved in the beam and the target typically used is 1 μm thick and therefore quite robust. It yields a rate of $R_{\mathrm{Det}} = I_{\mathrm{Det}}/e = 1.9\,\mathrm{kHz}$ per μA of primary current (I_0). For 3.5 MeV beam the effective analyzing power is $S_{\mathrm{eff}} \approx 0.38$ which results in a statistical FOM $S_{\mathrm{eff}}^2 I_{\mathrm{Det}}/I_0$ of only $9 \cdot 10^{-11}$, but due to the high primary currents the measurement time for better than 1% statistical accuracy is less than 1 min, at least for currents in the microampere range.

The device is routinely used by the accelerator operators. Since the deflecting magnet is not optimized for low hysteresis the re-optimization of MAMI takes about half an hour, therefore the usual rate of measurements is once per day. This is sufficient to observe drifts of the beam polarization which can happen due to the change of the photocathode surface in the polarized source. Since the usual rate of polarization change is less than 1% per day the effect on the experimental results can be taken into account by such Mott measurements with sufficient precision.

The polarimeter achieves reproducible and consistent results with a maximum of 1% peak to peak variation for primary currents varying by three orders of magnitude, see Fig. 9.

The device was analyzed for the three main sources contributing to systematics, which are the theory error of the Sherman function, uncertainty of extrapolation to foil thickness zero, and the dilution by backgrounds. The first two have already been discussed above. For the specific case of the Mainz Mott the contribution of the background was simulated by GEANT4 and was found to be on the order of

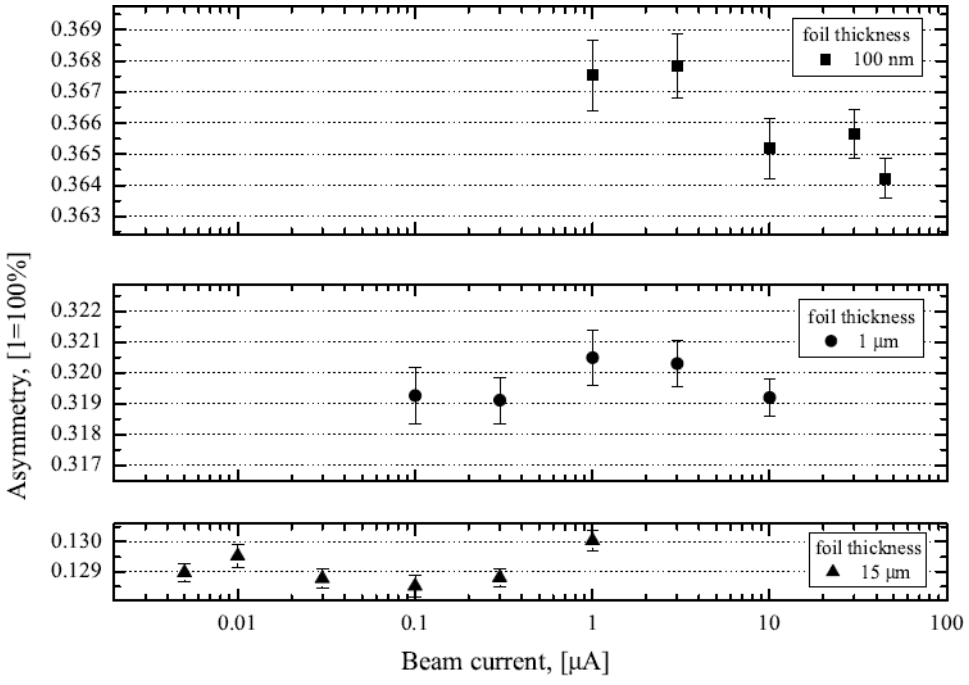

Fig. 9. Asymmetries as a function of primary current. Figure from Ref. 39. Variable target thicknesses are used to limit the count rate.

1%. It is therefore believed that an absolute calibration of the polarimeter at the 1% uncertainty level can be achieved with reasonable additional effort.

2.3. *Summary*

Mott polarimetry has been demonstrated to be extremely useful for the characterization of electron beam sources, providing absolute polarization measurements at keV and MeV energy scales. Measurements at few MeV energies can achieve high precision (better than 1%) with short measurement times. The major source of systematic uncertainty, the effective Sherman function, is under better control at MeV energies. Furthermore, extensive experimental studies of the "zero-thickness" extrapolated Sherman function, in combination with numerical modeling, suggest that this source of systematic uncertainty is under control.

3. Møller Polarimetry

Møller scattering is the elastic scattering of two electrons. Polarized electron scattering $\mathbf{e}^- + \mathbf{e}^- \rightarrow e^- + e^-$ provides large measurable asymmetries proportional to the beam and target polarizations. The first "Møller polarimeter" was developed in 1957 for $\sim$1 MeV electrons and positrons in order to study beta decays.[45] The first Møller polarimeter for ultra-relativistic electrons was built at the SLAC in

1975[1] and since then Møller polarimeters have been widely used at electron linear accelerators with polarized beams. Such a polarimeter consists of a target containing polarized electrons, and a spectrometer selecting the products of the scattering within a certain kinematic range.

3.1. *Polarized Møller scattering*

The Møller cross-section in the center-of-mass (CM) frame depends on the projections of the beam and target polarization vectors $\mathbf{P}^{\mathrm{b}}$ and $\mathbf{P}^{\mathrm{t}}$:

$$\frac{d\sigma}{d\Omega^*} = \frac{d\sigma_\circ}{d\Omega^*} \cdot \left[1 + \sum_{i,j=x,y,z} P_{\mathrm{i}}^{\mathrm{b}} A_{\mathrm{ij}} P_{\mathrm{j}}^{\mathrm{t}}\right]. \tag{10}$$

The process is calculable in the leading order of Quantum electrodynamics (QED). In the ultra-relativistic approximation the unpolarized cross-section is[46]

$$\frac{d\sigma_\circ}{d\Omega^*} = \frac{\alpha^2}{s} \frac{(3+\cos^2\theta^*)^2}{\sin^4\theta^*}, \tag{11}$$

where $s = 2m_e(E_\circ + m_e)$ is the Mandelstam variable, θ^* is the scattering angle in CM, and $E_\circ$ is the beam energy in the frame where the target particle is at rest. Assuming that the beam direction is along the Z-axis and that the scattering happens in the ZX plane, in the ultra-relativistic approximation[47,48]:

$$A_{ZZ} = -\frac{\sin^2\theta^* \cdot (7+\cos^2\theta^*)}{(3+\cos^2\theta^*)^2}, \quad A_{XX} = -\frac{\sin^4\theta^*}{(3+\cos^2\theta^*)^2}, \quad A_{YY} = -A_{XX},$$
$$A_{ZX} = A_{XZ} = -\frac{2\sin^4\theta^*\cos\theta^*}{\gamma(3+\cos^2\theta^*)^2}, \quad A_{XY} = A_{YX} = A_{ZY} = A_{YZ} = 0, \tag{12}$$

where $\gamma = \sqrt{s}/2m_e$. The dependence of the unpolarized cross-section and the analyzing power A_{ZZ} on the scattering angle in CM is shown in Fig. 10. At $\theta^* = 90°$

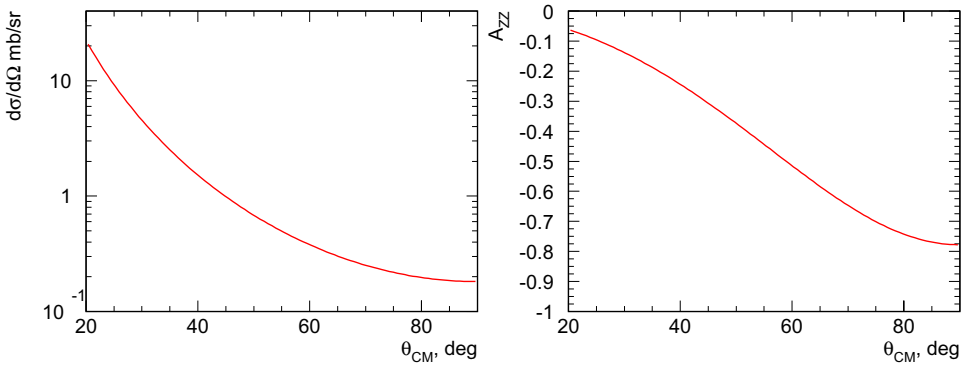

Fig. 10. The differential cross-section in the CM frame for $E_{\mathrm{LAB}} = 1\,\mathrm{GeV}$ (left) and the longitudinal analyzing power A_{ZZ} (right) as a function of the CM scattering angle.

the analyzing power has its maximum: $|A_{ZZ\ \max}| = 7/9, |A_{XX\ \max}| = 1/9$. The A_{XZ} value is suppressed by the γ-factor as well as $\cos\theta^*$ at $\theta^* \sim 90°$. Typically, the purpose of the polarimeter is to measure the longitudinal component of the beam polarization. The impact of the transverse components has to be minimized and/or accounted for.

The analyzing powers have also been calculated for arbitrary beam energy.[47] In the nonrelativistic case $\sqrt{s} \to 2m_e$, at $\theta^* = 90°$, $A_{ZZ} = A_{XX} = A_{YY} \to -1$. With increasing energy the values of the asymmetries asymptotically approach the approximation of Eq. (12):

$E_\circ$, GeV	0.05	0.10	0.20	0.40
$A_{ZZ}(E_\circ)/A_{ZZ}(\infty)$ at 90°	1.0026	1.0013	1.00065	1.00032.

The radiative corrections to the Møller analyzing powers have been calculated.[49,50] The expected effect may reduce the average analyzing power by 0.2–1.0% relative, depending on the acceptance of the particular polarimeter[50] to inelastic scattering. Acceptance uncertainties may result in ∼0.5% uncertainties in the analyzing power.

3.2. *Measurement techniques*

3.2.1. *Polarized targets*

So far, Møller polarimeters have used magnetized ferromagnetic materials as a source of polarized target electrons. They provide an electron polarization of 7–8%. Such targets are relatively simple to build and operate. They also have certain limitations. Target heating by the beam changes the magnetization. This limits the electron beam current to a few μA, while some of the experiments which depend on the polarization measurements run at higher beam currents, e.g., 100 μA. Typical targets are thick enough to be mechanically stable, but affect the electron beam and therefore make the polarization measurement invasive. On the positive side, a 1% statistical uncertainty of the measurement can be achieved in 3–30 min — a relatively short time.

Properties of ferromagnetic materials. At the magnetic saturation of pure iron about two electrons out of six populating the d-shell of the atom are spin-polarized. However, the exact degree of polarization is not calculable theoretically and has to be derived from magnetic measurements. One has to know the magnetization of the target in the area hit by the beam. The spin and the orbital contributions to the magnetization of the particular ferromagnetic material are determined by gyromagnetic experiments.[51] These experiments measure the gyromagnetic factor $g' = \frac{2m_e}{e}\frac{dM}{dJ}$, where M is the magnetization of the material and J is the angular momentum per unit volume. The spin-driven contribution M_S to the magnetization can be extracted since the gyromagnetic factors for the orbital and the spin

contributions differ by the electron's g-factor, $g \approx 2.002$: $\frac{M_S}{M} = \frac{(g'-1)g}{(g-1)g'}$. Knowing the magnetization, M, one can derive the average spin polarization of the electrons in the material:

$$P = M\frac{(g'-1)g}{(g-1)g'}\frac{1}{N_e g\mu_B/2} = M\frac{(g'-1)2}{(g-1)g'}\frac{1}{N_e\mu_B}, \tag{13}$$

where $N_e = N_A \cdot \rho \cdot Z/A$ is the density of the electrons in the material and μ_B is the Bohr magneton. For example, the magnetization of iron at 294 K in a 1 T external field was measured[52] $M/\rho = 217.7 \pm 0.2$ emu g^{-1} $= 217.7$ A m^{-1}kg^{-1} m^3. The measured gyromagnetic factor for iron is $g' = 1.919 \pm 0.002$.[53] The measurements were done at relatively low magnetization of less than 10% of the saturation value, and at room temperature. Using the iron properties $A = 55.845$ and $Z = 26$ one obtains $P = 8.003 \pm 0.011\%$. Extrapolation from 1 T external field to full saturation increases the magnetization by about 0.2%.[54]

In order to maximize the polarization and minimize the uncertainties the target material should be close to saturation. A thin ferromagnetic foil can be magnetized close to saturation in relatively low fields (10–30 mT) parallel to its surface, however the result may strongly depend on the quality of the material and on the annealing procedure.

Levchuk Effect.[55] The effective target polarization observed by the Møller polarimeter may differ from the average polarization of Eq. (13). The correlation between the momentum and the polar angle of the scattered electron offers a convenient way to reduce the acceptance to various backgrounds. However, such a correlation is smeared out if scattering happens from the electrons of the inner shells of the atom, which have energies that are not negligible compared to the CM energy. This may lead to a different acceptance for scattering from the polarized (outer) electrons and the unpolarized (inner) ones. This effect changes the effective polarization of the target, and requires a correction which can reach several percent relative. Some early polarimeter implementations led to effects as large as 14%.[56]

In-plane magnetized ferromagnetic foils. Most Møller polarimeters[1,57–63] have used, or are planning to use ferromagnetic foils 10–100 μm thick oriented at a small angle ($\sim 20^\circ$) to the beam and magnetized along its surface ("in-plane") by a field of 8–30 mT parallel to the beam. Typically, only the longitudinal beam polarization is measured, but a transverse component of the target polarization allows one to measure the transverse beam polarization as well. Ferromagnetic alloys such as Supermendur (49% Fe, 49% Co, and 2% V) were typically used since they reach magnetic saturation at lower fields than iron. The magnetization of the foil was measured with the help of a pickup coil around the foil. The measurements depend on the variations of the foil thickness and its magnetic properties along its surface. The deeper the magnetic saturation of the foil, the less dependent the magnetization

is to the value of the field, temperature, and various nonuniformities of the foil. Experiments have claimed target polarization uncertainties of 1.5–3.0% relative.

Out-of-plane magnetized ferromagnetic foils. In a different scheme, a pure iron foil 2–10 μm thick is oriented perpendicular to the beam and is magnetized to saturation by a 3–4 T field perpendicular to its surface ("out-of-plane").[64] In such a condition the foil is considered fully saturated and the magnetization of the sample is not measured but taken from the existing bulk measurements of pure iron — the most studied ferromagnetic material. The polarization uncertainty of the fully saturated iron is estimated to be ∼0.2%. Additionally, a 0.06% uncertainty was associated with the target heating.[65] A 3° angular misalignment of the target with respect to the field direction would reduce the longitudinal target polarization by ∼1% at 3 T and ∼0.2% at 4 T.[64] Overall, a 0.25% relative uncertainty of the target polarization at 4 T was reported.[65]

3.2.2. *Spectrometers and event selection*

Møller polarimeters use magnetic spectrometers and collimators in order to detect the scattered electrons in the kinematic range of interest $\theta^* \sim 90°$ ($\theta \sim \sqrt{2m/E_\circ}$, $E \sim E_\circ/2$ in the Lab frame), while not deflecting the primary electron beam. Typically, the collimators select the scattering plane within a certain range of the azimuthal angle, and the magnets spread the electrons according to their momenta. In the two-body reaction, the momentum and the polar angle of each scattered particle are correlated. This correlation is smeared out by multiple scattering in the target and the Levchuk effect (see Sec. 3.2.1). The collimator and detector geometry is designed to accept scattering events matching this expected correlation to reduce the detected background.

If the experiments at a given linear accelerator use different beam energies, the polarimeter has to operate at different beam energies as well. This complicates the polarimeter optics. Typically, the elements — the target, the collimators, the magnets, and the detectors — are stationary in space, while the magnetic fields are optimized for the given beam energy.

The detectors must operate at a relatively high rate, therefore fast detectors such as plastic scintillators are typically used. Electromagnetic calorimeters are also used, allowing suppression of the low energy background. This background comes from the electromagnetic interactions of the electron beam with the polarimeter target. The secondary particles make electromagnetic showers in the elements of the beam line and can irradiate the detectors. Typically, the detector has to be well shielded from all directions apart from the path of the Møller-scattered electrons. The main high energy background comes from the radiative Mott scattering on the target nuclei, which will mimic Møller scattering when the scattered electron gets about half of the beam energy. Some polarimeters (for example at SLAC[61]) detected only one scattered electron. These single-arm polarimeters are sensitive to the backgrounds from radiative Mott scattering, which may contribute ∼10% of the

counting rate. The background subtraction is a source of an additional systematic error. Detecting both scattered electrons in coincidence allows reduction of the background to negligible levels.

The detectors measure the counting rates for two opposite beam helicities, and the asymmetry is calculated. The average analyzing power is calculated using Eq. (12) and the acceptance of the polarimeter. As shown in Fig. 10, the scattering analyzing power only weakly depends on the scattering angle in the vicinity of $\theta^* \sim 90°$. Therefore, the systematic error associated with the acceptance uncertainty is typically small.

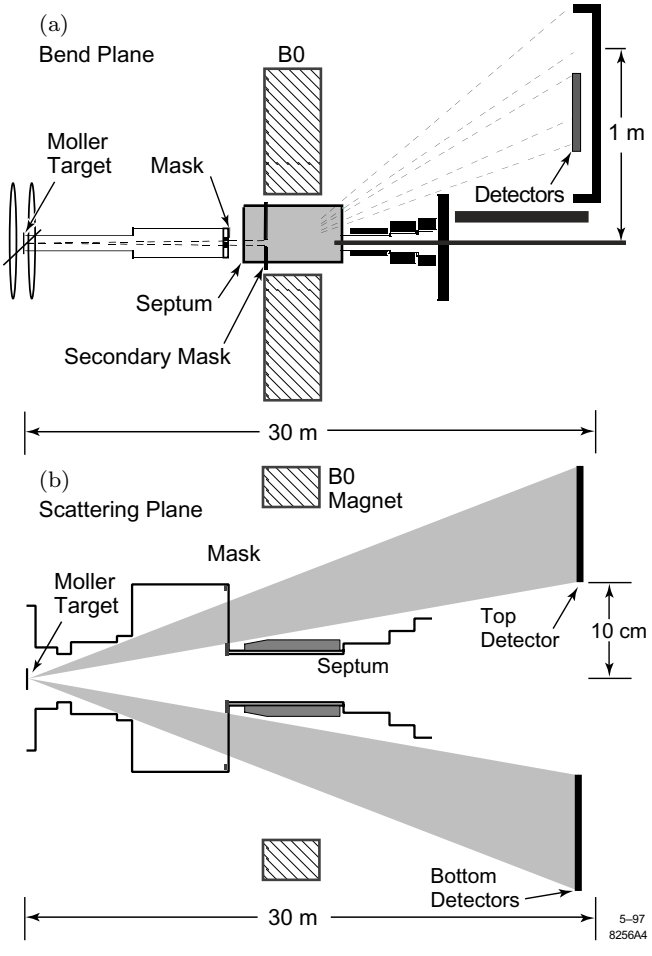

Fig. 11. The SLAC E154 Møller polarimeter: (a) top view; (b) side view. The mask was a disk with vertical slits of 0.2 rad opening. The Møller electrons crossed two narrow stripes in the detector plane. The stripes were slightly tilted from the horizontal direction due to the $\theta - p$ correlation. The top detector was segmented in the direction perpendicular to the stripe. Figure from Ref. 60.

3.3. *Møller polarimeters*

3.3.1. *SLAC*

After the development of the polarized electron beam and Møller polarimetry at SLAC[1] in 1975, the technique was used in a high-impact experiment[7,66] measuring electroweak effects. For this experiment, a 5% relative systematic uncertainty was attributed to the beam polarization measurements in which single-arm polarimetry and Supermendur target foils were used. Single-arm polarimeters were also used at SLAC for other experiments including SLD[56] at the beginning of the 1990s (which used the Linac Møller polarimeter), and polarized DIS experiments later (which used a Møller polarimeter in End Station A). Figure 11 shows the single-arm Møller polarimeter[60] used in End Station A for experiment E-154.

The two arms of the polarimeter were not used in coincidence because of the low duty cycle of the SLAC accelerator. Several Supermendur foils of different thicknesses (20–154 μm) were installed at 20° to the beam and magnetized (in-plane) in a longitudinal field of 10 mT. The secondary particles were collimated and deflected by a large magnetic dipole (the beam area was magnetically shielded). Silicon strip detectors with a 2.18 mm pitch covered the width of the Møller stripe. A lead radiator installed in front of the detector multiplied the number of electrons hitting the detector by a factor of ∼10.

The signals from the detectors were separately recorded for the two opposite helicities of the beam pulses (R and L). The combination $(R + L)$ contains the Møller peak and the background, presumably unpolarized (see Fig. 12, left).

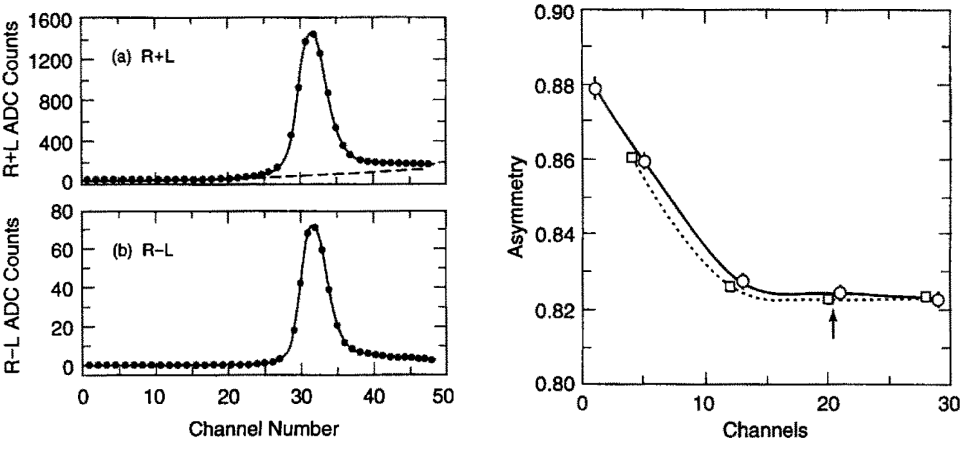

Fig. 12. The SLAC E154 Møller polarimeter results. Left: the profile of the signals on the strip detectors, (a) unpolarized $(R+L)$, consisting of the Møller peak and the background; (b) polarized $(R - L)$ — the unpolarized background cancels out. Right: the dependence of the measured asymmetry on the width of the detector used — demonstrating the Levchuk effect at smaller widths. The two calculated curves and two sets of symbols represent the top (high granularity) detector and the bottom (lower granularity) detector. Figures from Ref. 60.

Table 2. SLAC E154 Møller polarimeter[60]: contributions to the relative systematic error of the beam polarization measurements.

Uncertainty contribution	Value
Target polarization	1.7%
Analyzing power	0.3%
Background subtraction	2.0%
Acceptance and Levchuk effect	0.3%
Total	2.7%

The combination $(R - L)$ cancels the unpolarized background. The background level B was evaluated for the $(L + R)$ sample and the asymmetry calculated as $\frac{R-L}{R+L-B}$. Figure 12, right demonstrates the Levchuk effect — the measured asymmetry depends on the width of the Møller stripe used.

The systematic uncertainties for the SLAC E154 Møller polarimeter are summarized in Table 2. The dominant contributions come from the target polarization and background subtraction.

The same device was later re-configured into a two-arm polarimeter,[61] which measured the coincidence rate between the two arms. Due to the 10^{-4} duty cycle of the accelerator the instantaneous rates in the arms were ∼100 MHz. The spectrometer configuration was not changed, but the silicon detector was replaced by a multi-channel electromagnetic calorimeter. This led to a 2.4% overall systematic error, dominated by a 2.3% error on the target polarization.

3.3.2. *MAMI*

Figure 13 shows the two-arm Møller polarimeter[57] (1990) at MAMI, Mainz. Reference 57 describes the polarimeter tests carried out before the start of operation of the 850 MeV polarized CW beam. The tests used a pulsed, polarized beam in the energy range of 70–350 MeV in the single-arm mode, and an unpolarized CW beam in the coincidence mode. The target was made of Supermendur foils 6–20 μm thick, tilted at 30° to the beam, and magnetized in 6.5 mT field. Several foil orientations allowed measurement of the perpendicular component of the beam polarization. A relative error of 2% was attributed to the target polarization. The total relative systematic error was 9%.[67] This polarimeter was operated at MAMI from 1991–1998, and was replaced in 2001 by a device operating in the A1 hall of MAMI. This new polarimeter operates with an out-of-plane polarized target and two-arm detection with a dipole separation scheme. The relative accuracy was determined to 1.6%.[16,68]

3.3.3. *Bates*

Figure 14 shows the Bates two-arm Møller polarimeter[58] (1992). Due to a 1% duty cycle of the machine, the polarimeter was used in the single-arm mode. The background was evaluated by scanning the current in the quadrupole magnet. The

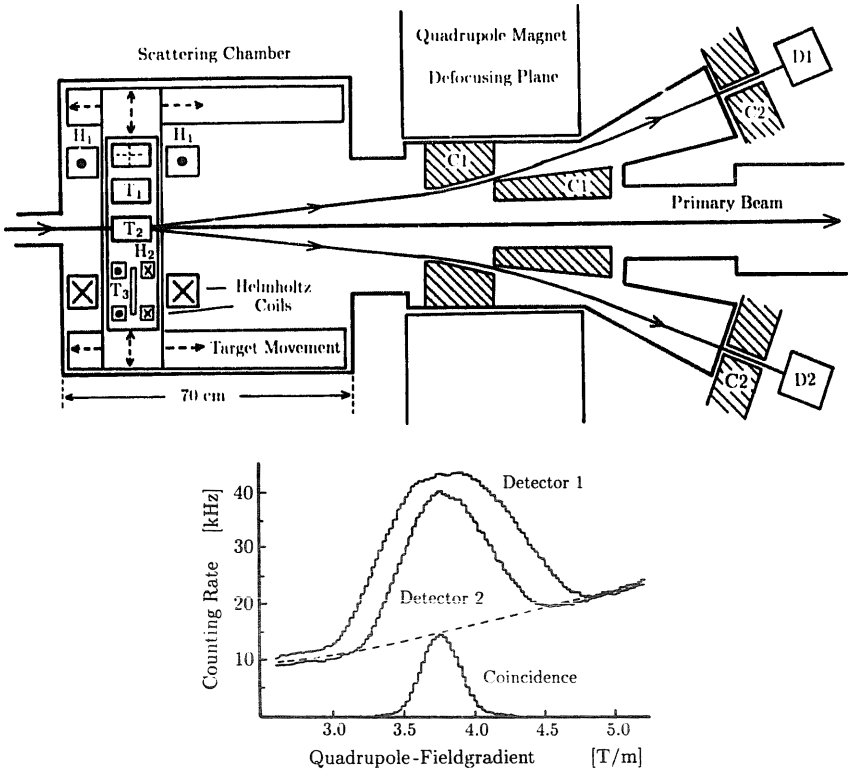

Fig. 13. The Møller polarimeter at MAMI, Mainz. Left: layout of the polarimeter. The quadrupole magnet deflected the Møller electrons away from the beam, through a system of collimators. Two Lucite Cherenkov detectors were used. Right: the Møller peak in the single-arm and in the coincidence modes. Figure from Ref. 57.

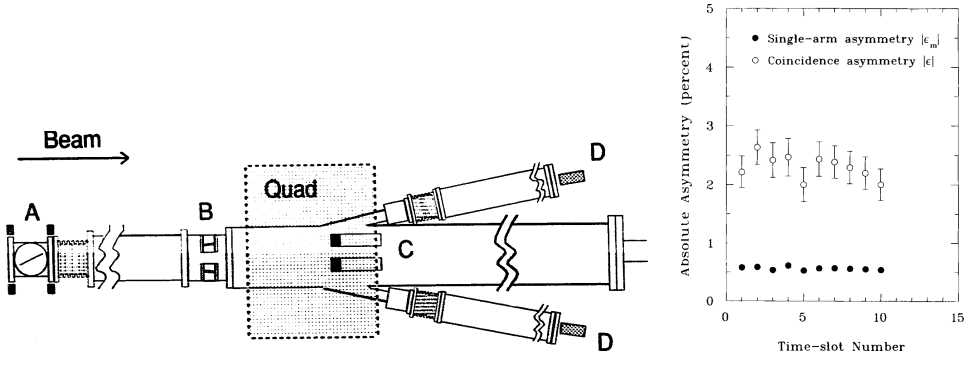

Fig. 14. The Bates Møller polarimeter. Left: the layout of the polarimeter. The target foil (A) was inclined at 30° to the beam. In order to adjust for different beam energies the vacuum had to be broken and the collimator (B) had to be moved manually. The quadrupole magnet (25 cm diameter) deflected the Møller electrons away from the beam. Two aerogel Cherenkov detectors were used. Right: the single-arm and the coincidence asymmetries measured at different phases of the powerline cycle. No dependence on the phase has been observed. Figures from Ref. 58 (left) and Ref. 59 (right).

Table 3. The Bates Møller polarimeter[58]: contributions to the relative systematic error of the beam polarization measurements.

Contribution	Value
Target polarization	1.25%
Target angle	2.1%
Beam position fluctuations	1.0%
Helicity-correlated beam shift	1%
Background asymmetry	5.0%
Total	6.0%

dominant error of ∼5% was associated with the background subtraction. For part of the measurements a 10% error was caused by a helicity-correlated beam shift. The target angle uncertainty added a 2.1% error. The systematic errors are summarized in Table 3.

The polarimeter was later re-configured into a two-arm coincidence device.[59] Lucite Cherenkov detectors were used. The overall systematic uncertainty was reduced to 2.9%. The Levchuk effect was not considered.

3.3.4. *ELSA*

The two-arm Møller polarimeter[69] (2004) at ELSA, Bonn, used one dipole magnet similar to the SLAC design, but no collimator was used, which minimized the Levchuk effect. The target foils made of a ferromagnetic alloy similar to Supermendur were magnetized in 35 mT longitudinal field. A relative error of 1.9% was attributed to the target polarization. The total relative systematic error was 1.9–2.0%.

3.3.5. *Jefferson lab*

Three experimental halls at Jefferson Lab (JLab) were equipped with Møller polarimeters. These polarimeters operated in the energy range of 0.85–6 GeV, and were upgraded later to operate at higher energies of 2–11 GeV.

Hall A. Figure 15 shows the Hall A (JLab) two-arm Møller polarimeter.[62,70] This polarimeter used quadrupole magnets to send the Møller electrons scattered close to the horizontal plane through two vertical slits in a dipole magnet, which deflected the electrons down toward the detector. The selection of the momenta and the angle was partially decoupled, which allowed reduction of the Levchuk effect. The detectors consisted of electromagnetic calorimeters with scintillator counters in front. The polarimeter used two types of targets: the traditional in-plane polarized foils made of iron and Supermendur, and the out-of-plane polarized iron foils. The results of the beam polarization measurements and the studies of systematic uncertainties are presented in Fig. 16: (top) for the in-plane and (bottom) for the out-of-plane polarized foils. The magnetization of the in-plane polarized foils was measured along the length of the foil[70] in order to correct for the foil nonuniformity. A set of beam

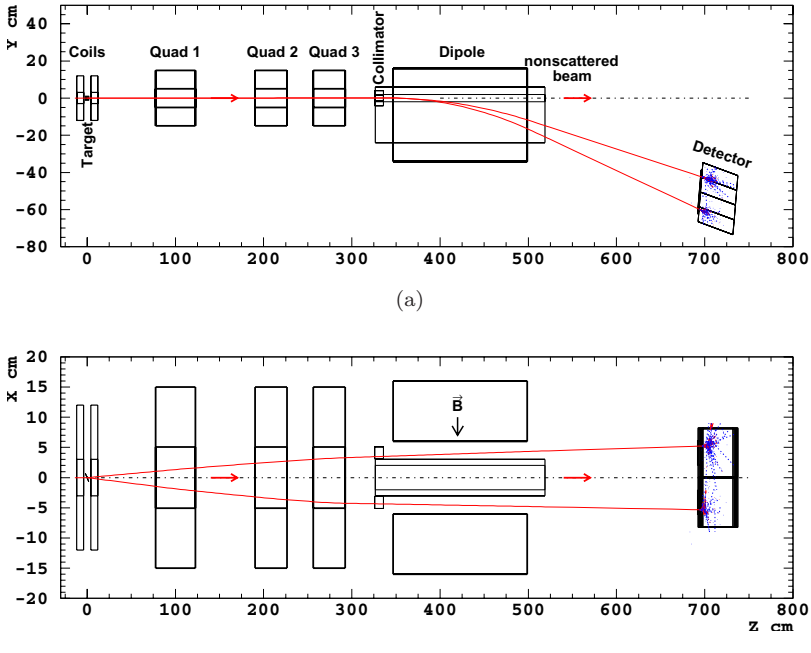

Fig. 15. The JLab Hall A Møller polarimeter[62,70]; (a) side view, (b) top view.

polarization measurements done with four different in-plane polarized foils shows a spread of the results. This spread, along with other factors, was used in the evaluation of the systematic uncertainty of the target polarization. The out-of-plane polarized targets provided a smaller foil-to-foil spread. In this case, an applied field of 3.5–4 T was needed to reach magnetic saturation, somewhat higher than claimed before.[64] It is known that the saturation curve depends on the purity of the material and the angle between the foil plane and direction of the magnetizing field. The systematic errors are summarized in Table 4.

Hall B. The two-arm Moller polarimeter in Hall B[71] used permendur foils magnetized in a 10 mT field, a spectrometer with two quadrupole magnets, and electromagnetic calorimeters for the detectors. The systematic error attributed to the target polarization was 1.4%, while the total systematic error was <3% relative.

Hall C. Figure 17 shows the Hall C two-arm Møller polarimeter.[65] This polarimeter pioneered the use of a target made of pure iron foils with saturated magnetization. Here, the foils were 2–10 μm thick and magnetized out-of-plane in a 4 T field. The foil saturation depends on the external field, on the angle of the foil plane with respect to the field direction, and on the temperature of the foil (see Fig. 18). The spectrometer uses a two-quadrupole optics that allows one to operate the polarimeter with the same tune for all beam energies. A set of movable collimators between the two quadrupoles allows for the reduction of Mott backgrounds without

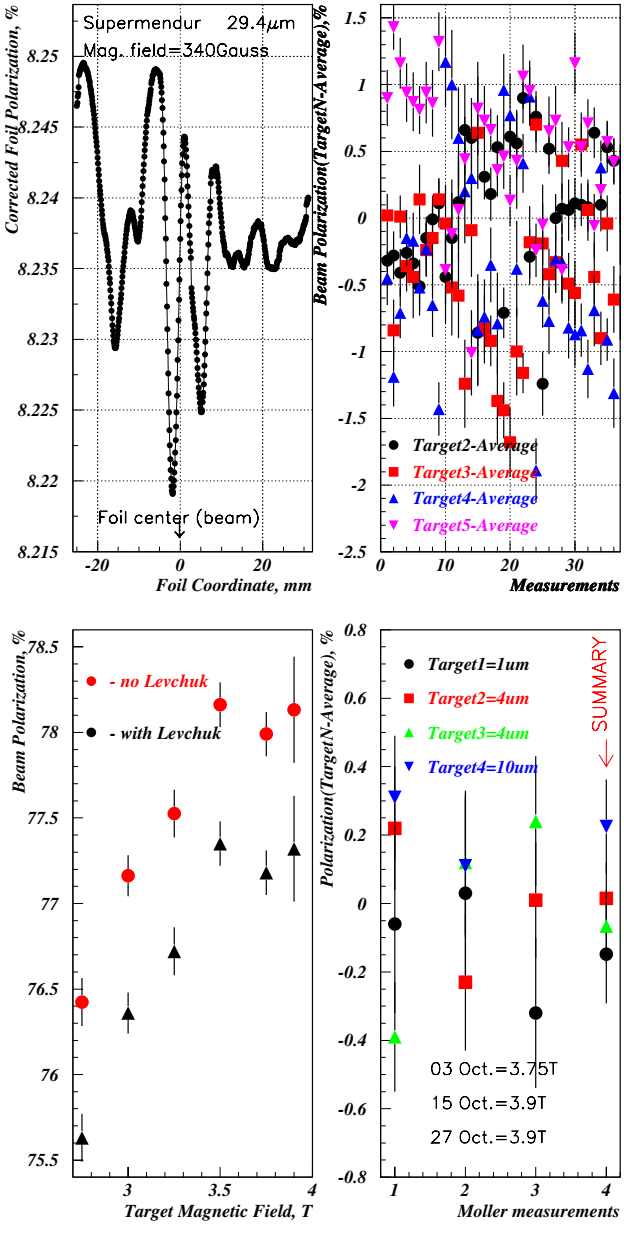

Fig. 16. The JLab Hall A Møller polarimeter: studies of the systematic errors. (Top) In-plane polarized foils: left — the foil polarization measured along the foil in the area hit by the beam; right — the deviations of the beam polarization measured with four different foils from the average values. (Bottom) Out-of-plane polarized foils: left — the beam polarization measured at different magnetizing fields, with and without the Levchuk correction; right — the deviations of the beam polarization measured with four different foils from the average values. Figures from Ref. 70 with kind permission of Società Italiana di Fisica.

Table 4. The JLab Hall A Møller polarimeter[70]: contributions to the relative systematic error of the beam polarization measurements. The "Others" contribution represents the observed variations of the measurement done at different times, which could not be explained by changes in the injector/accelerator configurations.

Contribution	Target polarization	
	In-plane	Out-of-plane
Target polarization	1.5%	0.35%
Analyzing power	0.3%	0.3%
Levchuk effect	0.2%	0.3%
Target temperature	0.02%	0.02%
Background	0.3%	0.3%
Dead time	0.3%	0.3%
High/low beam current	0.2%	0.2%
Others	0.5%	0.5%
Total	1.7%	0.88%

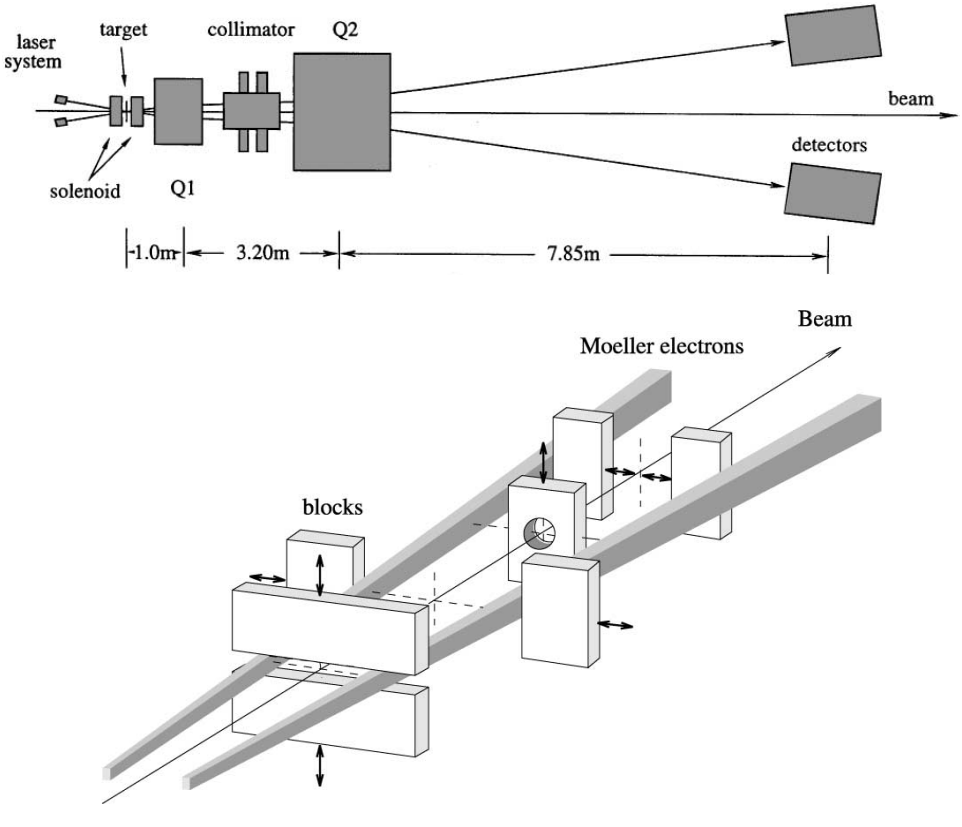

Fig. 17. The JLab Hall C Møller polarimeter (left) and the collimator layout (right). Figures from Ref. 65.

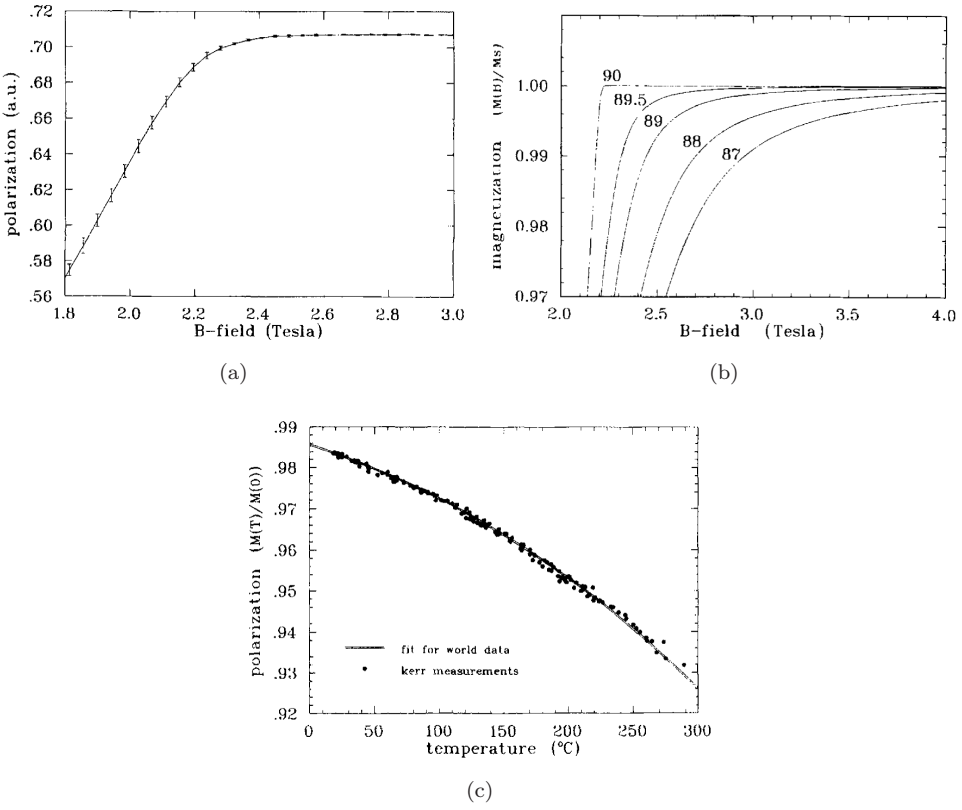

Fig. 18. The JLab Hall C Møller polarimeter: foil magnetization in transverse field. (a) measured saturation curve; (b) calculated dependence of the magnetization on the angle of the foil to the field; (c) measured dependence on the temperature. Figures from Ref. 64.

impacting the acceptance for the Møller electrons. The detector system consists of a pair of calorimeters for the main asymmetry measurement with segmented scintillators for verification and optimization of the polarimeter optics.

Due to the small uncertainty of the target polarization this is the most accurate Møller polarimeter constructed and used so far. The systematic uncertainties summarized in Table 5 represent the uncertainty of the device for a particular measurement at low current. In application for experiments, some uncertainty due to use of the low-current measurements for high-current data as well as interpolation between measurements results in slightly larger total uncertainties. Nevertheless, in either case, the total uncertainty is dominated by the correction due to the Levchuk effect and the target polarization. The authors of Ref. 65 neglected the anomalous magnetic moment of the electron, which would introduce a $\sim$0.2% bias. The uncertainty due to the target heating was given for a $\sim 1\,\mu$A current, although measurements have been made up $\sim 10\,\mu$A in conjunction with a beam rastering system; no change in measured asymmetry (at the $\pm 0.5\%$ level) was observed at

Table 5. JLab Hall C Møller polarimeter[65]: the uncertainties of various correction factors and contributions to the relative systematic error of the beam polarization measurements. These uncertainties represent an idealized situation in which no extrapolation to higher currents or interpolation between measurements is required.

Source	Uncertainty	Effect A(%)
Beam positions and directions	0.5 mm, 0.15 mr	0.16
Spectrometer magnetic field		0.12
Multiple scattering	10%	0.12
Levchuk effect	10%	0.30
Collimator position	0.5 mm	0.06
Target temperature	50%	0.05
Direction B-field	2°	0.06
Value B-field	5%	0.01
Spin polarization in iron		0.25
Total		0.47

these higher currents. There was also a plan to evaluate the effect of heating *in situ* using the Kerr effect, but no further results have been reported.

3.4. *Summary*

Parameters of several polarimeters are summarized in Table 6. The typical statistical uncertainty is much lower than the systematic one. The main limitations to the systematic accuracy come from the ferromagnetic targets due to the polarization uncertainty and the Levchuk effect. Such targets also make the measurements invasive to the "customer" experiment, and often have to be done at a much lower beam current, which may introduce additional systematic uncertainty. On the other hand, the uncertainties associated with the analyzing power of the Møller scattering are typically small.

The use of pure iron foils polarized out-of-plane by large applied magnetic fields has allowed a significant reduction in the overall systematic uncertainty, resulting

Table 6. Møller polarimeters.

Polarimeter	Beam energy (GeV)	Arms	Optics	$(dP/P)_{\text{syst}}$ Target	$(dP/P)_{\text{syst}}$ Full
SLAC[60]	48	1	D	1.7%	2.7%
SLAC[61]	16, 29	2	D	2.3%	2.4%
MAMI[57]	0.850	2	Q	2.0%	9.0%
MAMI[16,68]	0.850–1.50	2	D	0.6%	1.6%
Bates[58]	0.250, 0.574	1	Q	1.25%	6.0%
Bates[59]	0.868	2	Q	1.5%	2.9%
ELSA[69]	1.0–3.3	2	D	1.9%	2.0%
JLab, A[70]	0.85–6	2	QQD	1.5%	1.7%
JLab, A[70]	0.85–6	2	QQD	0.35%	0.9%
JLab, B[71]	0.85–6	2	QQ	1.4%	3.0%
JLab, C[65] (ideal)	0.85–6	2	QQ	0.3%	0.5%
JLab, C[72] (Q-Weak)	1.16	2	QQ	0.3%	0.8%

in Møller polarimeter measurements with <1% uncertainties. Future experiments requiring knowledge of the beam polarization of about than 0.5% will be challenging, although feasible, with existing devices. The most significant systematic uncertainty to address would be the Levchuk effect. It is possible that the use of higher precision electron wave functions could help reduce this source of uncertainty. The effect can also be measured for certain polarimeter configurations as has been demonstrated at SLAC.[60] An additional uncertainty may come from a dependence of the gyromagnetic factor g' on the magnetization, since the measurements have been done far from saturation. This potential uncertainty should be clarified. The acceptance of the polarimeter should be understood at a high accuracy, since both the Levchuk effect and the radiative corrections depend on it.

4. Compton Polarimetry

Compton polarimetry takes advantage of the well-known QED interaction between electrons and photons to extract electron beam polarization. Typically, a Compton polarimeter employs a laser that collides nearly head-on with the high energy electron beam. The resulting scattered photon is boosted to high energy in the backward direction. The polarimeter can detect the backscattered photon, scattered electron, or both. A clear advantage of Compton polarimetry is the fact that it is "nondestructive", and allows simultaneous measurement of the beam polarization under the same conditions and at the same time as the main experiment. Indeed, Compton polarimetry is typically the only viable form of beam polarimetry for storage rings which require minimum disruption to avoid negative impacts on the stored beam lifetime.

On the other hand, Compton polarimetry presents certain challenges when compared to other techniques. At fixed target accelerators with modest beam currents (μA scales), it is difficult to make rapid measurements using commercially available lasers. In addition, the analyzing power is strongly dependent on the beam energy

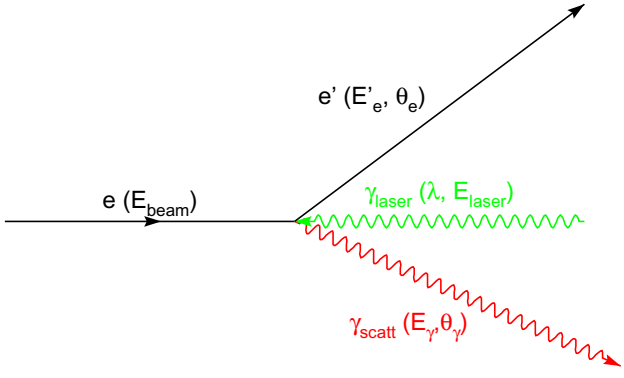

Fig. 19. Compton scattering.

which impacts both the FOM as well as the technique's flexibility. Even at fixed beam energy, the analyzing power has a strong dependence on the backscattered photon (scattered electron) energy.

4.1. *Kinematics, cross-section, and asymmetry*

In this section, we briefly review the kinematics and cross-sections for Compton scattering from high energy electron beams. This process is described in detail in several papers, including Refs. 73–76, the discussion here uses the formalism as presented in Refs. 77 and 78. Assuming an electron beam with energy E_e, colliding head-on with a laser system of wavelength λ such that the laser photon energy is $E_{\text{laser}} = hc/\lambda$ (see Fig. 19), the resulting scattered photon energy, E_γ, is given by

$$E_\gamma \approx E_{\text{laser}} \frac{4a\gamma^2}{1 + a\theta_\gamma^2\gamma^2}, \tag{14}$$

where θ_γ is the angle of the scattered photon relative to the incident electron direction, $\gamma = E_e/m_e$, and a is a kinematic factor defined

$$a = \frac{1}{1 + 4\gamma E_{\text{laser}}/m_e}. \tag{15}$$

The dimensionless quantity $\rho = E_\gamma/E_\gamma^{\max}$ is often used, with $E_\gamma^{\max} = 4aE_{\text{laser}}\gamma^2$. Note that the scattered electron energy, $E_e' = E_e + E_{\text{laser}} - E_\gamma$, is a minimum when $E_\gamma = E_\gamma^{\max}$.

The unpolarized differential cross-section for Compton scattering is

$$\frac{d\sigma}{d\rho} = 2\pi r_o^2 a \left[\frac{\rho^2(1-a)^2}{1-\rho(1-a)} + 1 + \left(\frac{1-\rho(1+a)}{1-\rho(1-a)} \right)^2 \right], \tag{16}$$

where r_o is the classical electron radius. The longitudinal analyzing power for polarized electrons and circularly polarized photons is

$$A_{\text{long}} = \frac{\sigma^{++} - \sigma{-+}}{\sigma^{++} + \sigma^{-+}} = \frac{2\pi r_o^2 a}{(d\sigma/d\rho)}(1-\rho(1+a)) \left[1 - \frac{1}{(1-\rho(1-a))^2} \right], \tag{17}$$

where σ^{++} (σ^{-+}) denotes the cross-section for electron and photon spins aligned (anti-aligned). In the case of transversely polarized electrons, the analyzing power depends on the azimuthal angle of the outgoing photon relative to the (transverse) polarization direction of the electron (ϕ),

$$A_{\text{tran}} = \frac{2\pi r_o^2 a}{(d\sigma/d\rho)} \cos\phi \left[\rho(1-a) \frac{\sqrt{4a\rho(1-\rho)}}{(1-\rho(1-a))} \right]. \tag{18}$$

While Compton polarimetry has been used to measure the transverse polarization of electron beams in storage rings, the technique relies on measuring the spatial dependence of the asymmetry, hence high precision is difficult to achieve.

The unpolarized cross-section and longitudinal analyzing power are shown in Fig. 20. These figures assume a 532 nm (green) laser colliding with electron beams

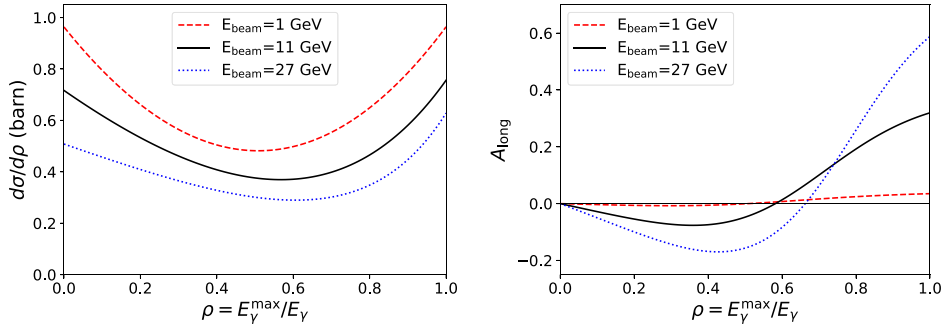

Fig. 20. Unpolarized Compton cross-section (left) and longitudinal analyzing power (right) assuming a 532 nm wavelength laser colliding with an electron beam at 1 GeV, 11 GeV, and 27 GeV.

from 1 GeV to 27 GeV. The unpolarized cross-section shows only a modest dependence on beam energy, while the longitudinal analyzing power changes rather dramatically. At the kinematic endpoint, $E_\gamma = E_\gamma^{max}$, the analyzing power grows from 3.5% at 1 GeV to 58.8% at 27 GeV.

4.2. *Apparatus and measurement techniques*

The key components required for a Compton polarimeter are a laser system and a detector for either the backscattered photon or the scattered electron. The requirements on these components depend on the accelerator in which the polarimeter is deployed. A cartoon of a "generic" Compton polarimeter is shown in Fig. 21.

4.2.1. *Laser system*

The choice of laser system depends crucially on the accelerator environment. Storage rings generally operate at high average electron beam current (on the scale of mA) so that rapid polarization measurements can be made using commercial lasers operating at ∼1–10 W. In addition, typical storage ring bunch structures (short bunches at relatively low repetition rates) mean that low average power lasers operated in

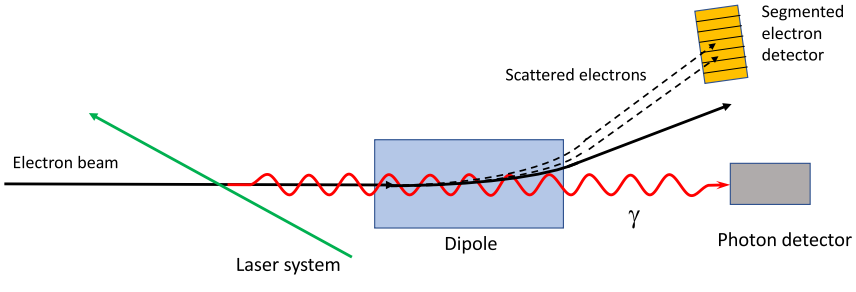

Fig. 21. Key components in a Compton polarimeter including the laser system, photon detector, and electron detector. One or more steering magnets are required to deflect the electron beam away from the photon detector as well as momentum analyze the scattered electrons.

pulsed mode result in high instantaneous luminosities, which in turn lead to a built-in suppression of beam-related backgrounds (primarily Bremsstrahlung radiation). In this case, the polarimeter must be operated in "multiphoton" mode, which will be discussed later.

Fixed target machines (Jefferson Lab, MAMI) generally operate at much lower average currents (scale 1–100 μA) such that commercial lasers generally provide insufficient power to yield rapid polarization measurements and result in poor signal to background ratio. A solution to this challenge was first suggested in Ref. 79 which proposed the use of narrow linewidth lasers (with power of order 1 W) coupled to a high-finesse (and high-gain) Fabry–Pérot resonating cavity to provide intracavity powers approaching 10 kW. The electron beam makes use of this stored power by colliding with the laser beam at the center of the cavity. This technique was first employed in experimental Hall A at Jefferson Lab[80,81] and later in Hall C,[82] as well as in HERA at DESY.[83] A novel modification of this technique was also used in the A4 Compton at Mainz.[84]

4.2.2. *Photon detector*

The type of detector required for detection of the backscattered photon is a strong function of the beam energy as well as measurement technique. For example, the longitudinal polarimeter at HERA[85] operated at a beam energy of 27 GeV resulting in a maximum backscattered photon energy of 13 GeV (532 nm laser). However, since the device measured many backscattered photons from one beam bunch, the total energy deposited could be on the order of thousands of GeV. In this case $NaBi(WO_4)_2$ crystals, 19 radiation lengths long, were used. For this application, resolution was less important than containing the shower and maintaining good linearity.

On the other hand, at 1 GeV beam energies, the maximum backscattered photon energy is only 34 MeV. At these energies, crystals such as NaI, CsI, or GSO are more appropriate, providing sufficient energy resolution to precisely measure the backscattered photon energy spectrum.

Polarimeters aimed at measuring the transverse polarization must also have some sensitivity to position since they must measure an up–down (typically) asymmetry. This position sensitivity could be via a tracking detector or a multi-crystal calorimeter-type detector.

4.2.3. *Electron detector*

Measurement of the scattered electron is typically only employed in longitudinal polarimeters. A segmented detector placed after one or more dipoles allows momentum analysis of the scattered electron and reconstruction of the Compton spectrum. The position resolution depends on the geometry of the polarimeter as well as the beam energy. Highly segmented silicon and diamond strip detectors (pitch

≈200 μm) have been employed at Jefferson Lab[80,82] whereas the SLD polarimeter[86] at the SLAC Linear Collider (SLC)[86] used a segmented Cherenkov detector with each channel about 1 cm wide.

Since the electron detector is employed primarily for tracking or position measurements, the polarization measurement systematics are dominated by knowledge of the system dispersion and detector geometry, rather than the detailed detector response, as is the case for the photon detector.

4.2.4. *Measurement techniques*

The polarization can be extracted in several ways. The most intuitive is the "differential" measurement; in this case the energy of the backscattered photon (or scattered electron) is determined event by event and an experimental asymmetry versus energy spectrum is determined. The theoretical analyzing power is then fit to the measured asymmetry spectrum to determine the polarization.

The polarization can also be determined by extracting the "energy weighted" asymmetry. The detector integrates the total energy deposited for a given electron (or photon) helicity state, and the asymmetry is formed from this integrated energy measurement. This technique has the advantage of a larger analyzing power and decreased sensitivity to the low energy part of the spectrum.

Polarimeters that operate in "multiphoton" mode, in which many backscattered photons are detected per bunch, must operate in energy integrating mode. An exception to this is the SLD Compton polarimeter[86]; in this case, the segmentation of the Cherenkov electron detector provides the Compton spectrum energy information, but each channel of the detector provides a signal proportional to the number of scattered electrons in each bunch via the size of the Cherenkov signal.

Several Compton polarimeters and their measurement techniques (as well as other properties including laser system, operating beam energy, and systematic uncertainties) are listed in Table 7.

4.3. *Previous and existing Compton polarimeters*

4.3.1. *Transverse polarimeters*

Early Compton polarimeters were used exclusively at storage rings where they are the most practical method for making direct measurements of the beam polarization. Initial applications employed Compton polarimeters to track the degree of transverse polarization and demonstrate the "self-polarization" of electron beams in storage rings due to the spin-dependent emission of synchrotron radiation (the Sokolov–Ternov effect[87]).

As seen in Eq. (18), the analyzing power for Compton scattering from transversely polarized electrons varies as the azimuthal angle of the scattered photon. For vertically polarized electrons in a storage ring, this yields an up–down asymmetry. The first Compton polarimeter was used at the SLAC e^+e^- storage ring, SPEAR.[88]

Table 7. Compton polarimeters including nominal operating energies and performance. Not all Compton polarimeters are included in the table — an emphasis has been placed on those used to provide absolute beam polarization measurements.

Polarimeter	Beam energy	Laser wavelength and technology	Detection and method	Sys. uncertainty (dP/P)	References
CERN LEP	46 GeV	532 nm (pulsed)	γ/integrating	5%	99, 100
HERA LPOL	27.5 GeV	532 nm (pulsed)	γ/integrating	1.6%	85
HERA TPOL	27.5 GeV	514 nm (CW)	γ/counting	2.9%	92, 101
MIT-Bates	0.3–1 GeV	532 nm	γ/counting	6%	95, 96
NIKHEF	<1 GeV	514 nm	γ/counting	4.5% @ 440 MeV	94
Mainz A4	0.85,1.5 GeV	514 nm intra-cavity Ar–ion	(γ,e)/counting	N/A	98
JLab Hall A	1–6 GeV	1064 nm, FP cavity	γ/counting	3% (2002)	81
			e/counting	1% (2006)	102
			γ/integrating	1% (2009)	103
	1.1 GeV	532 nm, FP cavity	γ/integrating	1.1% (2010)	104, 9
JLab Hall C	1.1 GeV	532 nm, FP cavity	e/counting	0.6%	82
			γ/integrating	3%	105
SLD at SLAC	45.6 GeV	532 nm (pulsed)	e/multiphoton	0.5%	86, 106

This polarimeter used a cavity-dumped Ar–Ion laser (514.5 nm) pulsed at a frequency matched to the ring circulation frequency. The laser collided with 2.7–3.7 GeV positrons, and a position sensitive photon detector about 13 m downstream of the collision point was used to determine the up–down Compton asymmetry. Spectra from the SPEAR Compton are shown in Fig. 22. Similar Compton polarimeters were constructed at DORIS-II[89] and VEPP-4[90] at Novosibirsk, the Cornell Electron Storage Ring (CESR),[91] LEP at CERN,[92] and HERA (TPOL) at DESY.[92] More recently, measurements with a transverse Compton polarimeter at ELSA[93] have been attempted, although polarization results have not yet been obtained. In several cases, the transverse Compton polarimeter measurements are more relevant for measurements of the storage ring energy via resonance depolarization than for determination of the absolute beam polarization. Because the analyzing power depends crucially on the position calibration of the scattered photon detector, and because the backscattered photons are emitted in a rather small cone, it is difficult to achieve high precision with this flavor of Compton polarimeter. For example, LEP and HERA achieved about 5% and 3% systematic uncertainties (dP/P), respectively.

4.3.2. *Longitudinal polarimeters*

In this section, we discuss longitudinal Compton polarimeters at storage rings, as well as the A4 Compton polarimeter at Mainz (fixed-target). We defer discussion of the SLD and Jefferson Lab Compton polarimeters to the next section.

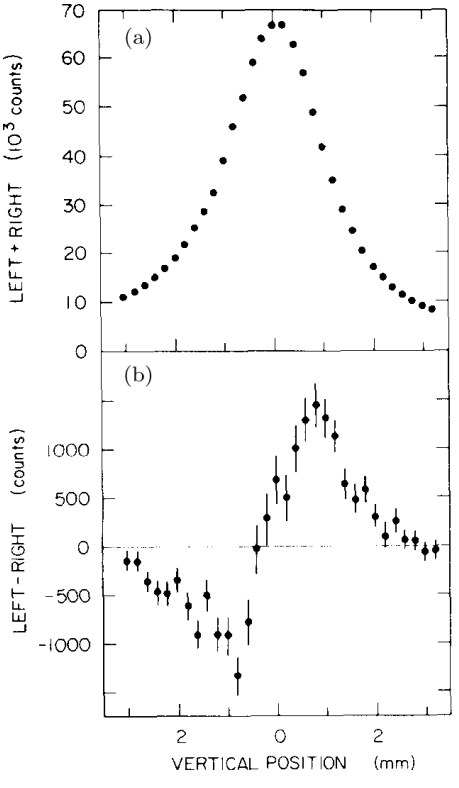

Fig. 22. Laser helicity sum (top) and difference (bottom) spectra from the SPEAR Compton photon detector at a beam energy of 3.6 GeV. The laser polarization was flipped between left and right helicities and the yield and difference distributions versus vertical position were measured. Figure from Ref. 88.

The longitudinal Compton polarimeter (LPOL)[85] at HERA ($E_{\text{beam}} = 27.5\,\text{GeV}$) was located downstream of the HERMES experiment and made use of a pulsed (100 Hz), frequency-doubled Nd:YAG laser at 532 nm. The large peak power of the laser resulted in many backscattered photons per laser-beam collision, hence the device was operated primarily in multiphoton mode. The photon detector consisted of four $NaBi(WO_4)_2$ crystals and the resulting systematic uncertainty of 1.6% was dominated by determination of the detector response.

An additional longitudinal polarimeter[83] was later installed downstream of the original HERA LPOL. This polarimeter made use of a 1064 nm Nd:YAG laser coupled to a high-gain Fabry–Pérot cavity yielding several kW of stored power. A new sampling photon calorimeter was also constructed and the resulting system, which operated in counting mode, achieved a systematic uncertainty of 1%.

The longitudinal polarization has been measured via Compton polarimetry in lower energy storage rings as well. The AmPS ring at NIKHEF (with electron beam energies up 900 MeV) installed a Compton polarimeter with a CW

Ar–ion laser (514 nm) and a pure CsI crystal to detect the backscattered photons in event mode.[94] A systematic uncertainty of 4.5% (dP_e/P_e) was achieved at $E_{\text{beam}} = 440\,\text{MeV}$. It is of note that this was the first time a Compton polarimeter measured the longitudinal polarization of an electron beam in a storage ring.

The Compton polarimeter at MIT-Bates[95,96] used many of the lessons learned at NIKHEF and also used a green CW laser (5 W at 532 nm) along with a CsI crystal to detect the backscattered photons. A 6% (dP_e/P_e) systematic uncertainty was achieved at a beam energy of 850 MeV.

As noted earlier, Compton polarimeters at fixed-target facilities are difficult to employ due to the typically low beam intensity ($I_{\text{beam}} \sim 1$–$200\,\mu\text{A}$) compared to colliders ($I_{\text{beam}} \sim \text{mA}$), resulting in unworkably long measurement times. At Jefferson Lab, this was overcome with the use of external, high-gain Fabry–Pérot cavities, resulting in ∼kW of stored laser power. The Mainz A4 Compton polarimeter[84,97,98] employed a novel variation of the cavity technique. In this case, the cavity of the laser itself was extended (by moving the output coupler) and the electron beam impinged on the laser light stored in the internal laser cavity. The advantage of this technique is that a complicated feedback system would not be necessary to keep the cavity on resonance. While the stored power is lower (scale 100 W rather than kW), the power was high enough to enable measurements in times on the order of hours rather than days. The Mainz A4 Compton polarimeter used a NaI crystal to detect the backscattered photons and a scintillating fiber array to detect the scattered electrons. The final systematic uncertainty for this device has not yet been reported.

4.4. *High precision Compton polarimetry*

Since the Compton scattering process is pure QED, there is no fundamental limit on the level of precision that can be achieved. However, the experimental challenges are often significant. As discussed earlier, the excellent control of the detector position in measuring the up–down asymmetry in measurements of transverse beam polarization has led to systematic uncertainties of a few percent. Measurement of the longitudinal polarization poses certain advantages, but the challenges are still significant. In this section, we discuss Compton polarimeters that have achieved or have the potential, with modest improvements, to achieve systematic uncertainties significantly better than 1%.

4.4.1. *SLD Compton at SLAC*

The first sub-1% Compton polarization measurement was achieved using the polarimeter developed for the SLD experiment.[86] The SLD Compton polarimeter used a single-pass (pulsed) laser system; this made it relatively straightforward to monitor the laser polarization both before and after the interaction point. Scattered electrons were detected in a multi-channel gas Cherenkov detector. The Compton

endpoint analyzing power was large (≈75%) and the corresponding scattered electrons were located >10 cm from the nominal beam path. The absolute analyzing power was calibrated by scanning the detector across the scattered electron spectrum. The resulting systematic uncertainty was $dP/P = 0.5\%$.

4.4.2. *Hall A Compton at Jefferson lab*

The Hall A Compton polarimeter[80] makes use of a laser coupled to an external Fabry–Pérot cavity resulting in several kW of stored laser power. The laser system sits at the center of a 4-dipole chicane, with a photon and electron detector downstream of the third dipole. The laser polarization inside the cavity is determined by making measurements of the so-called "transfer function" which tracks the evolution of the laser polarization as it passes through the various birefringent elements needed to guide the laser into the beamline vacuum and cavity. The transfer function technique relies on detailed modeling of both the incoming and outgoing laser transport and is difficult to do with high precision. Historically, the laser polarization has been one of the more significant uncertainties in systems that employ Fabry–Pérot cavities.

The Hall A Compton polarimeter made use of a silicon strip detector for detection of the scattered electrons. 1%-level precision was achieved with this detector, but its utility was limited at energies below 3 GeV.

Initially, the Hall A Compton used a multi-crystal lead-tungstate array for detection of the backscattered photons. Recently, a GSO crystal (better suited to the few GeV beam energies common at Jefferson Lab) was installed.[103] In addition, a "threshold-less integration" technique was employed to minimize sensitivity to the absolute energy calibration of the detector. The "energy integrated" signal is sensitive primarily to knowledge of the detector linearity, which can be reliably determined via careful LED measurements. In addition, "threshold-less" analysis removes dependence on the absolute energy scale of the threshold that would be needed for a measurement of the differential energy spectrum. Rapid measurements of the asymmetry are made by comparing the energy-weighted signal integrated over a fixed period of time to a corresponding measurement with the opposite beam helicity. A histogram of these "helicity pair" measurements is shown for each laser polarization state in Fig. 23. This figure also shows measurements of the different detector response used to test the detector linearity.

4.4.3. *Hall C Compton at Jefferson lab*

Similar to the Jefferson Lab Hall A Compton polarimeter, Hall C also used an external Fabry–Pérot cavity to increase the flux of laser photons (in this case the FP cavity provided up to 2 kW of intra-cavity power at 532 nm). While measurements of the transfer function were performed to determine the laser polarization inside the cavity, the Hall C system employed a technique mentioned by the POL2000

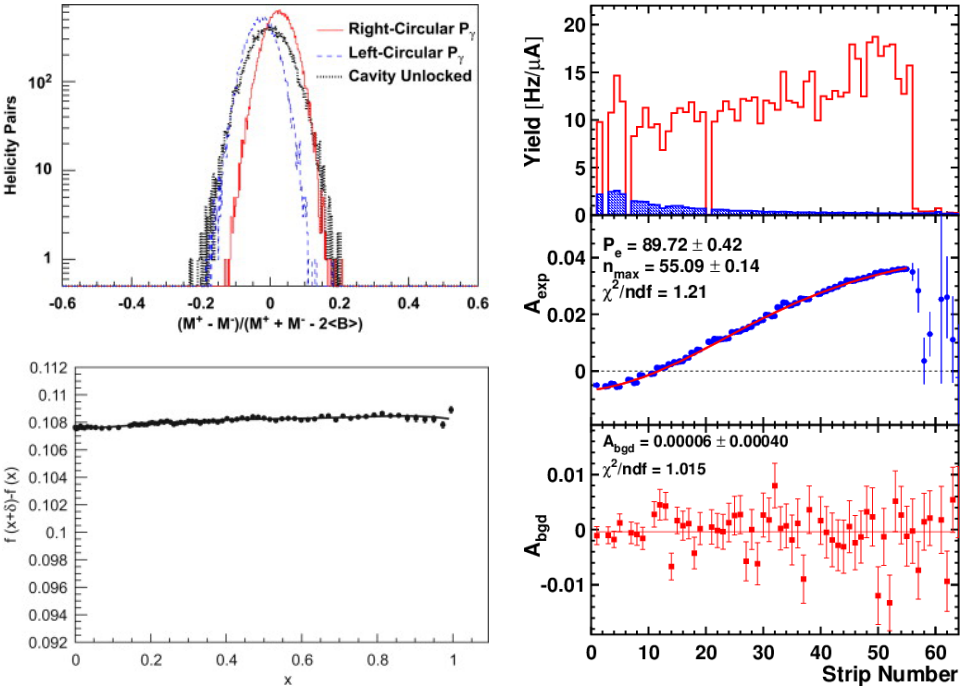

Fig. 23. Left: (Top) Energy-integrated asymmetry in the Hall A GSO photon detector for left and right circularly polarized laser light, as well as for laser-off background measurements. (Bottom): Finite-difference response as measured using a multi-LED pulser system with maximum amplitude resulting in a signal in the GSO equivalent to 200 MeV photons. Figures from Ref. 103 (top) and Ref. 107 (bottom). Right: Hit spectrum (top), asymmetry and fit (middle), and fit residuals (bottom) for Hall C Compton diamond-strip electron detector. Figure[108] from Ref. 82.

collaboration[109] at HERA and described in more detail in Ref. 110. The degree of circular polarization at the first mirror of the Fabry–Pérot cavity is inferred making use of optical reversibility theorems and by monitoring the light reflected from the cavity. Supplemental measurements of the polarization inside the cavity (with the vacuum system removed) were directly compared to the polarization signal obtained from the reflected light and found to be in excellent agreement (Fig. 24). This technique resulted in a systematic uncertainty of $<0.2\%$ for the polarization of the light stored in the cavity.

The Hall C polarimeter used a diamond strip detector after a momentum-analyzing dipole to detect the Compton-scattered electrons. The fine segmentation of the detector ($200\,\mu$m pitch) allowed precise measurement of the asymmetry spectrum. The polarization was extracted via a 2-parameter fit of the asymmetry spectrum (varying the beam polarization and the kinematic endpoint) which minimized sensitivity to knowledge of the absolute position of the detector relative to the beam. An example of hit-spectrum and fit is shown in Fig. 23.

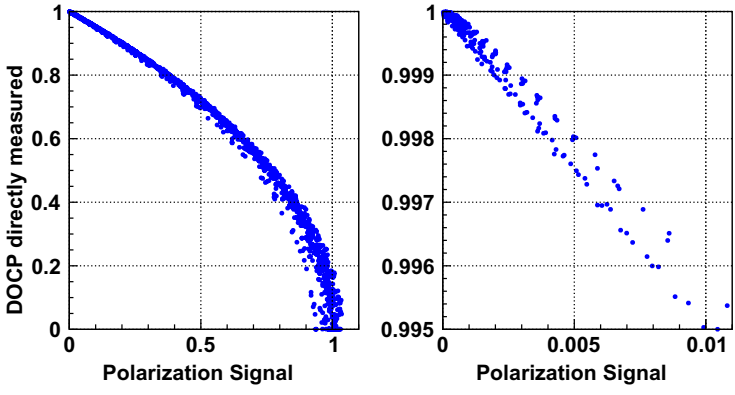

Fig. 24. Demonstration of technique used to monitor laser polarization inside the Hall C Compton Fabry–Pérot cavity. Direct measurements of the laser polarization inside the cavity (vertical axis) are compared to the signal obtained from laser light reflected back from the first cavity mirror. Figure[108] from Ref. 82.

4.4.4. *Comparison of precision Compton polarimeters*

A comparison of the SLD, Hall A, and Hall C Compton polarimeters is shown in Table 8. The top half of the table shows some of the properties of each polarimeter relevant to the eventual total systematic uncertainty. For example, the laser system used by the SLD Compton lent itself to straightforward precise determination of the degree of circular polarization at the interaction point, while the Fabry–Pérot cavities used in the JLab Hall A and C devices required more indirect determination of the laser polarization.

The second half of the table lists the systematic uncertainties for each device. In this case, we have taken the detailed systematic uncertainty tables for each, and recast them into broader, more generic categories. For example, "detector response" encompasses determination of the linearity of the Cherenkov response for SLD,

Table 8. Comparison of properties and systematic uncertainties of high precision Compton polarimeters (SLD,[86,106] JLab Hall A[103] and JLab Hall C[82]).

	SLD	Hall A (photon)	Hall C (electron)
Properties			
Beam energy	45.6 GeV	3 GeV	1.16 GeV
Endpoint A_{long}	74.7%	5.21%	4.06%
Laser system	532 nm, pulsed	1064 nm, FP cavity	532 nm, FP cavity
Detector	Cherenkov	GSO	Diamond strip
Scheme	Multiphoton	Integrating	Differential
Uncertainties		dP/P (%)	
Laser polarization	0.10	0.80	0.18
Detector response (linearity, gain)	0.20	0.48	0.1
Analyzing power determination	0.40	0.13	0.27
DAQ and electronics related	0.20	N/A	0.48
Total	0.50	0.94	0.59

linearity and gain shifts for the Hall A GSO detector, and strip-by-strip efficiency for the Hall C diamond detector. "Analyzing power determination" includes all inputs necessary to calculate the theoretical asymmetry as measured by the detector; beam energy, geometric acceptance/dependence (collimator for Hall A, detector position for Hall C), magnetic elements in spectrometer-based systems, etc. Finally, "DAQ and electronics related" includes noise related to the SLD and Hall C electron detectors as well as dead-time and trigger-related inefficiencies in Hall C.

Each system has clear "high-nails" that, if addressed, would lead to improved precision. The largest uncertainty for the SLD Compton comes from determination of the analyzing power, which could be improved by increased detector segmentation and better modeling of the spectrometer.[111] The Hall A systematic uncertainty is clearly dominated by determination of the laser polarization inside a Fabry–Pérot cavity. While the Hall C system improved upon the laser polarization uncertainty, the dominant uncertainty in that case came from the DAQ, and in particular was related to inefficiencies (inadvertently) introduced by the FPGA-based readout.

The 12 GeV program at Jefferson Lab includes experiments that require electron beam polarimetry with precision better than 0.5%. While this has not yet been achieved at JLab, the results from the Hall A and Hall C Compton polarimeters suggest that goal is within reach. Applying the Hall C laser polarization optimization technique in combination the Hall A integrating-mode photon detection would result in a systematic uncertainty of 0.53%. Modest improvements in determination of the detector response would reduce the uncertainty further. The Hall C electron detector could be improved by straightforward improvements to the detector readout firmware. Reduction of the DAQ related uncertainty from 0.48% to 0.2%, for example, would result in a systematic uncertainty of 0.39%.

5. Direct Comparisons of Electron Polarimeters

The high precision demanded by future experiments poses a significant challenge for electron beam polarimetry. In this review, we have discussed multiple beam polarimetry techniques with an emphasis on the ever-improving systematic uncertainties achieved. However, while a particular device may claim a very high precision, it is crucial that this claim be checked by at least one other technique and/or device of comparable precision. When systematic uncertainties approach the level of 0.5%, there is little margin for error and seemingly small mistakes in the assessment of the device or its systematic uncertainty become relatively significant. Direct comparisons of multiple polarimeters can play a crucial role in achieving reliable, high precision polarimetry. In sections that follow, we will discuss some examples of direct comparisons of precision electron beam polarimeters.

5.1. *Spin dance*

In high energy accelerators the electron beam polarization experiences a cumulative precession, often by thousands of degrees, when traversing the electro-magnetic

fields of the particle accelerator between the electron source and polarimeter. Most facilities requiring precision measurement of the beam polarization host multiple polarimeters, at different locations and using different beam energies. As discussed in previous sections, each method of polarimetry measures either the longitudinal or a transverse component of the beam polarization. Typically, dedicated spin rotators are implemented to compensate for the total precession experienced. These spin rotators used near the source may add or subtract to the total precession to effectively orient or vary the beam polarization at any polarimeter in any desired orientation.

At Jefferson Lab a so-called Spin Dance has become a powerful tool to improve knowledge of a polarimeter analyzing power. In a spin dance, a single spin rotator near the electron source is used to vary the direction of the same polarized beam at all of the participating polarimeters, often simultaneously. The polarization orientation will in general be different at each polarimeter for a given spin rotator setting, but after varying the spin rotator over a broad range each polarimeter effectively maps out the same exact beam polarization (see e.g., Fig. 25). In spite

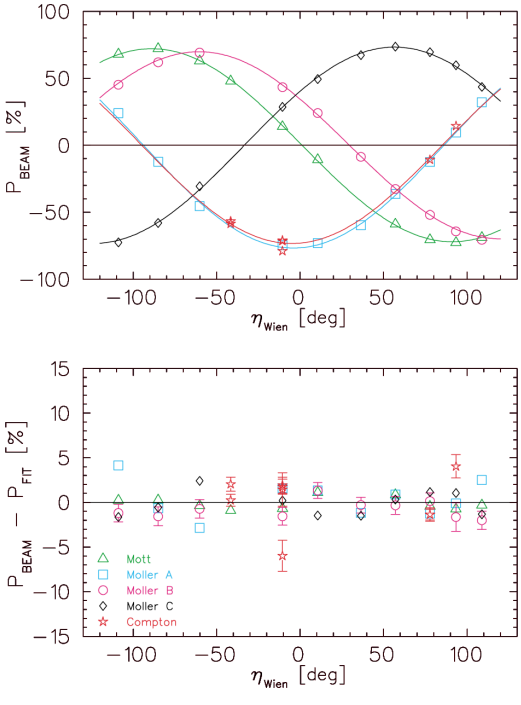

Fig. 25. Measured polarizations and fits (upper plot) relative to the Wien filter spin rotator. Fit residuals (lower plot), with only statistical uncertainties from the fits shown. In general, the uncertainties from the fits are smaller than the symbol sizes used in plotting the data.
Note: The lower plot legend applies to the upper plot. Figure[108] from Ref. 112.

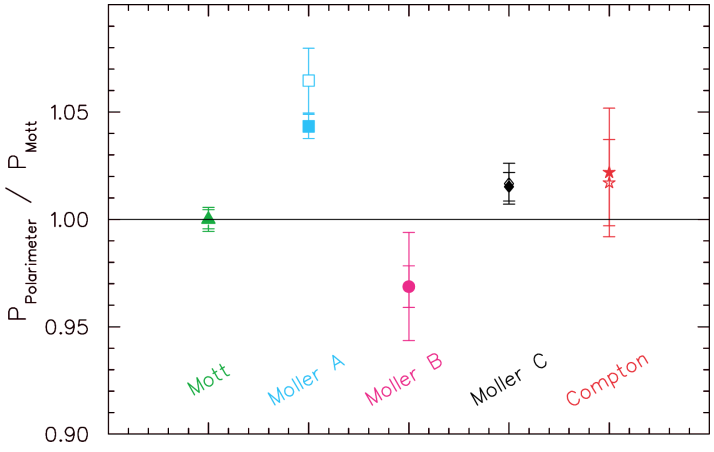

Fig. 26. The relative analyzing powers for the five Jefferson Laboratory electron beam polarimeters, normalized to the Mott polarimeter for comparison. The solid symbol markers represent the results for the dataset limited to be within 25% of the maximum measured polarization. Figure[108] from Ref. 112.

of the difference in precession incurred between the various polarimeters this technique provides a powerful method to compare the results of each polarimeter and allows one to test the presumed systematic uncertainties and reveal discrepancies.

In the case of Ref. 112, the results led to an improved understanding of the Hall A Møller polarimeter. Figure 26 compares the relative analyzing power of the five polarimeters studied when including only measurements in Fig. 25 within 25% of the maximum measured polarization with those without such a limitation. This comparison revealed a 2–3% systematic contribution of the transverse component of the beam polarization to the determination of the longitudinal component of the beam polarization at the polarimeter.

5.2. *Møller–Compton comparison at JLab, Hall C*

As part of several studies to verify the systematic uncertainties of the electron beam polarimeters in experimental Hall C at Jefferson Lab, a dedicated measurement was made to directly cross-check the beam polarization as measured by the Hall C Møller and Compton polarimeters. During the Q_{weak} experiment,[11,113] the Hall C Compton polarimeter typically operated at a beam current of 180 μA, while the Møller polarimeter made measurements at 1–2 μA. A test was performed during which both polarimeters made measurements, one right after the other, at the same beam current ($\approx$4.5 μA) in order to verify that both devices gave the same result under the same beam conditions.[114]

The results yielded good agreement within the respective uncertainties of the devices, although in this case the Compton polarimeter had a rather large statistical uncertainty (0.71%) due to operation at low beam current. An additional result of this test was that, when compared to nearby Compton measurements at high beam

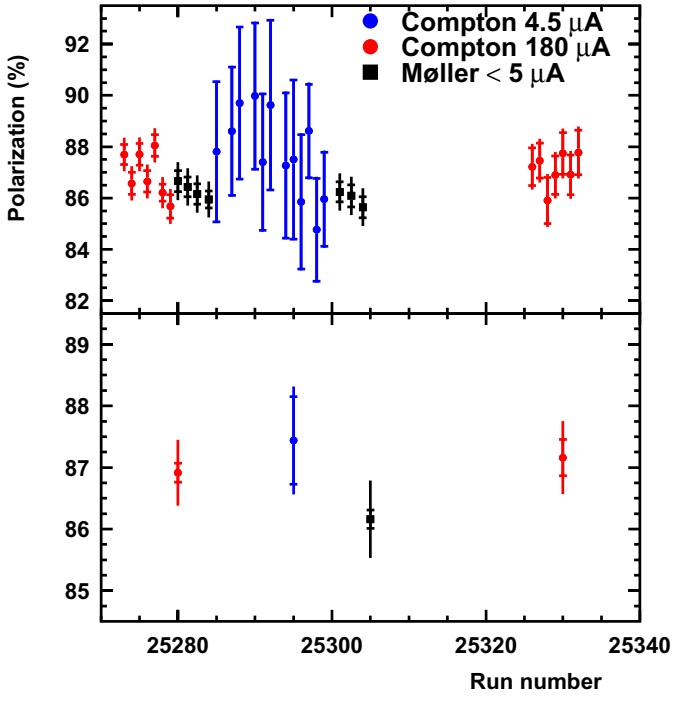

Fig. 27. (Color online) Comparison of Jefferson Lab Møller and Compton polarimeters in Hall C. Data were taken in the Møller and Compton at identical beam currents (black and blue points) and were found to agree. Comparison with high current Compton data and placed limits on the current dependence of the beam polarization. Figure[115] from Ref. 114.

currents, the polarization was shown to not depend on beam current (at the 1% level) over a current range of 175 μA. Results from the Hall C Møller–Compton comparison are shown in Fig. 27.

In addition to the dedicated test described above, the Q_{weak} experiment provided a large body of data from both the Hall C Compton and Møller polarimeters, taken at the polarimeters' respective nominal operating parameters. This dataset[82] included more than 20 measurements from the Møller polarimeter and nearly continuous running of the Compton polarimeter over several months. On average, the two devices were found to agree to better than 1%, with some variation due to time-dependent systematic uncertainties.

5.3. *Outlook*

Direct polarimeter comparisons have proven valuable for demonstrating polarimeter consistency at the 1% level. For experiments that require <0.5% precision at Jefferson Lab, further comparisons will be required. Within a single experimental hall (on the same beamline), these should include direct comparison of the quasi-correlated measurements from the Compton polarimeter electron and photon detectors, as

well as comparisons of Compton and Møller polarimeters. A next-generation Spin-Dance measurement, involving $dP/P < 1\%$ polarimeters in the injector (the Mott polarimeter) and experimental Halls A and C (Møller and Compton polarimeters) would also be an extremely powerful demonstration of the validity of the systematic uncertainties assigned to each device.

6. Further Developments in Precision Electron Polarimetry

In earlier sections, we have described the standard techniques most commonly used for measurements of electron beam polarization: Mott, Møller and Compton polarimetry. As the requirements of nuclear physics experiments have become more demanding, polarimetry techniques have become more precise to meet these needs. For the most part, the improvement in precision could be characterized as incremental modifications to techniques that have been in use for many years. Future experiments pose unique challenges with regards to precision and significant improvements to these existing techniques, as well as new methods are desired. In this section we will discuss some new approaches under development that, if successful, will result in more robust polarization measurements with improved systematic uncertainties.

6.1. *Atomic hydrogen Møller target*

The accuracy of Møller polarimetry is limited mainly by the use of ferromagnetic foils for the polarized electron target. A potential alternative to the ferromagnetic foil is atomic hydrogen gas. This gas can be stored in a cold magnetic trap at $\sim$0.3 K, which provides nearly 100% electron polarization. Such a target would remove the main sources of the systematic error: the target polarization and the Levchuk effect. Furthermore, such a target can potentially work at high beam current, providing continuous measurements during the experiment, while a ferromagnetic target requires special invasive measurements at low beam current. A detailed feasibility study[116–118] has been performed. While such traps have been used in particle physics experiments, they have not been used directly in a high-power charged particle beam. The potential depolarization effects can be kept under control at the 0.01% level, with certain modifications to the storage cell. It remains to be proven that such modifications would not affect the trap performance. Building such a target would require a limited R&D program, as well as considerable efforts and funding.

Such a program is ongoing at the University of Mainz where this type of polarimeter is foreseen for the P2 experiment. A detailed design of the atomic trap has been achieved and fabrication of the trap and its cryogenic environment has begun. Polarization measurements with the atomic hydrogen target are expected beginning in 2021.

Møller polarimetry with atomic hydrogen is particularly attractive in that it measures the polarization at or near the experiment and can potentially make

measurements at the same time as the main experiment. In the next sections, new approaches that measure the polarization at lower energies (at or near the accelerator injector) are discussed. While these approaches do hold promise for high precision, they would necessarily involve some additional uncertainty associated with applying that polarization to the experimental data (at higher energy).

6.2. *Electron spin optical polarimetry*

In electron spin optical polarimetry a spin-polarized electron beam excites a ground state noble gas atomic target to an upper triplet state via spin-exchange. Upon decay of this state to a lower triplet level, light emitted along the axis of the initial spin polarization is observed (Fig. 28). Due to spin-orbit coupling in the excited atomic state, the spin orientation of the incident electron is converted to orbital orientation, causing this light to be partially circularly polarized. If the atomic states involved are well-LS coupled and spectroscopically resolved, the circular polarization fraction can be related directly, by angular momentum algebra alone, to P_e. Generally speaking, one can show that

$$P_e = \frac{P_3}{a + bP_1}, \tag{19}$$

where a and b are determined by simple angular momentum coupling algebra and P_1 and P_3 are the relative Stokes parameters corresponding to linearly-polarized light (referenced to the incident electron beam axis) and to circularly-polarized light, respectively. If the excited states involved are not well–LS coupled, a and b must be determined using approximate dynamical calculations. In this case, the

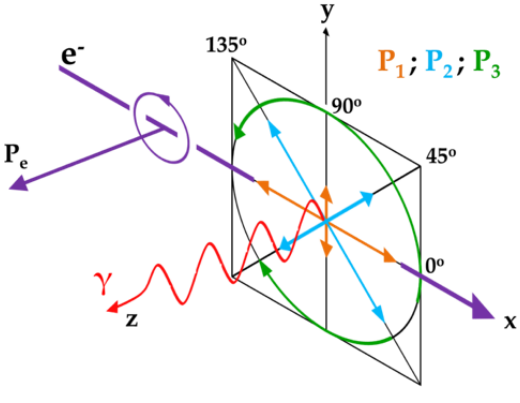

Fig. 28. (Color online) A typical geometry for electron optical polarimetry. Electrons having transverse polarization along the z-axis are incident on the target along the x-axis. Fluorescence is best detected along the direction of the electron spin. The relative Stokes parameters of the fluorescence are indicated schematically in the x–y plane with green arrows (circular polarization P_3), blue arrows (canted linear polarization P_2), and orange arrows (linear polarization P_1). Figure[119] reprinted with permission from Ref. 119. Copyright 2017 by the American Physical Society.

third Stokes parameter P_2, which is the linear polarization fraction referenced at $45°/135°$ to the beam axis, will be nonzero. Thus, the measurement of P_3 essentially determines P_e, the measurement of P_1 determines the polarimeter analyzing power, and a null check of P_2 establishes the validity of the method.

The optical polarimetric method has a number of important advantages, its chief one being that it is absolute. It also has higher analyzing power than, e.g., Mott scattering, varying from 50% for He targets to 70% for heavy noble gases. The main disadvantages of electron optical polarimeters are that they are inefficient and require very low-energy input beams. Typically, several nanoamperes of beam are required to ensure measurement times less than 10 min. Incident energies must correspond to those associated with atomic valence shell excitation, namely 10–20 eV. An example of typical optical polarization data taken with a Kr target[120] and an incident electron polarization $P_e = 26.00(14)\%$ (statistical) is shown in Fig. 29.

This method has been explored previously at MAMI[122,123] but most recently a program dubbed Accurate Electron Spin Optical Polarimetry (AESOP) is being pursued by the Nebraska group.[124,125] In this effort the goal of the Nebraska group is to measure optical polarization to a statistical accuracy of 0.1% and an overall accuracy of 0.4%. With such accuracy, AESOP opens a new pathway to test systematics of other polarimetry methods, e.g., by accelerating the same

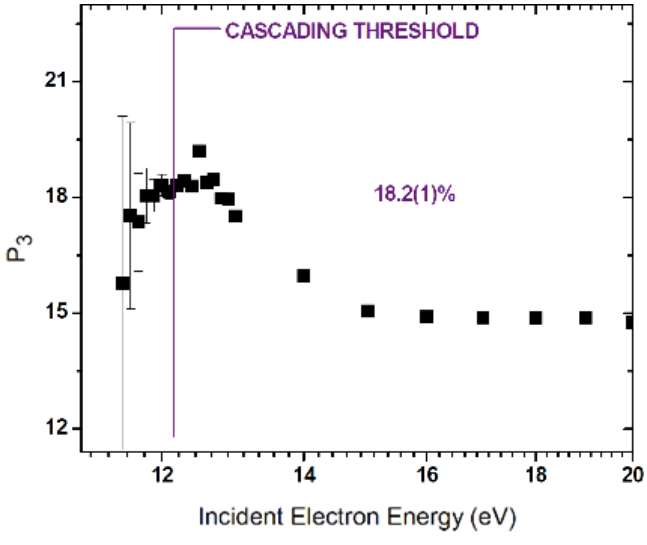

Fig. 29. The circular polarization relative Stokes parameter P_3 as a function of incident electron energy for the $5^3D_3 \rightarrow 4^3P_2$ 811 nm transition in Kr. The excitation threshold is at 11.4 eV. Above 12.2 eV, the electron can excite the $3d_3$ and higher levels that cascade into the 5^3D_3 state, invalidating Eq. (19). For data below the cascading threshold, P_3 is constant within statistical uncertainty, and is known with a statistical precision of 0.55%. The analyzing power for Kr is 0.700,[121] yielding $P_e = 26.00(14)\%$ (statistical error only).

electron beam polarization measured in the AESOP apparatus to a Mott scattering polarimeter.

6.3. *Double-Mott polarimeter*

A different approach toward high precision polarimetry is to use double scattering. The idea is to *measure* the effective analyzing power S_{eff} of a scattering experiment instead of trying to determine it. This approach distinguishes double scattering from all other polarimetry techniques. The method was thoroughly analyzed in a series of papers by the group of Prof. Kessler at the University of Münster/Germany.[126–128] The measurement works in the following way. A first elastic scattering from an unpolarized beam produces a polarized scattered beam with a vertical polarization $P_{\text{Scat}} = S_{\text{eff}}$. This polarization is in general lower than the theoretical analyzing power of the process S_0 due to the spin diffusion in the target of finite thickness. This creates several of the systematic errors in conventional Mott polarimetry whereas it is — at least in principle — not important in this case. The secondary beam is directed to an identical target where a scattering asymmetry is observed under the same angle as in the first scattering. Provided that the two scatterings — notably the targets — can be made identical, the observed asymmetry A_{obs} is given by

$$A_{\text{obs}} = S_{\text{eff}}^2. \tag{20}$$

After this procedure the targets are calibrated and each of them can be used to analyze a polarized beam with the effective analyzing power S_{eff}. Kesslers group used primary beam energies of up to 120 keV which cannot be extended to much higher energies due to the rapidly falling elastic cross-section. The method is therefore restricted to energies typical for polarized sources and is of course invasive.

The accuracy of this method is limited by several issues which were addressed in great detail in the papers cited. The most obvious ones are:

- Control of false asymmetries. The usual method of creating double ratios cannot be applied since the initial beam is unpolarized. The geometrical arrangement of the monitor counters which are needed to correct for, e.g., misalignments of the beam has to be handled with great care.
- The extent to which the targets can be made identical.
- Handling of backgrounds (Møller-scattering, multiple scattering, X-rays).

The systematic errors quoted in Ref. 127 for typical gold targets of surface density of $\approx 100\,\mu\text{g/cm}^2$ are $\Delta S_{\text{eff}}/S_{\text{eff}} = 0.6\%$.

Double scattering offers another attractive feature which may allow to reduce the systematic error even further if it is used also with a polarized primary beam. It was observed by Hopster and Abraham[129] that additional observables can be gained under this conditions. It is assumed that the initial vertical beam polarization can be flipped with the condition $P_0 \rightarrow -P_0$. The primary target is considered as an auxiliary target which no longer has to have the same effective analyzing power as

the second one (S_{eff}), but has a value S_T instead which also has to be determined from the measurements. The double scattering experiment with unpolarized beam now yields

$$A_1 = S_T S_{\text{eff}}. \tag{21}$$

One can also move the second target into the primary beam path, then observing

$$A_2 = P_0 S_{\text{eff}}. \tag{22}$$

Scattering on the first target with the two input polarizations $\pm P_0$ yields different secondary beam polarizations $P_{\uparrow,\downarrow}$ which depend on S_T but also on the depolarization factor of the auxiliary target α, a fact that was again observed in Ref. 128.

$$P_\uparrow = \frac{S_T + \alpha P_0}{1 + P_0 S_T}, \tag{23}$$

$$P_\downarrow = \frac{S_T - \alpha P_0}{1 - P_0 S_T}. \tag{24}$$

Taking this into account more asymmetries can be measured by double scattering:

$$A_3 = P_\uparrow S_{\text{eff}}, \tag{25}$$

$$A_4 = P_\downarrow S_{\text{eff}}. \tag{26}$$

While measuring A_3, A_4 one can also monitor the scattered beam current from the auxiliary target which is nothing else than the single scattering asymmetry:

$$A_5 = P_0 S_T. \tag{27}$$

One finds that the extension proposed in Ref. 129 implies considerable advantages:

- The five observations $A_1 \ldots A_5$ depend on the four unknowns S_T, S_{eff}, P_0, and α result in an over-defined system of equations hence allowing the extraction of the unknowns in five independent ways, providing systematic cross checks.
- The condition of identical targets is revoked, respectively replaced by the condition that the degree of spin polarization does not change during the spin flip $P_0 \rightarrow -P_0$, which can be done with high accuracy by the optical flip of the excitation light helicity at the source.

It was shown in Ref. 128 that the auxiliary target thickness can be varied by a factor eight without any observable influence on the extracted analyzing power of the second target at a level $<0.4\%$.

The apparatus of the Münster group was transferred to Mainz[130] where its applicability for the P2 experiment at the MESA accelerator is being tested. It

has been demonstrated that the mechanically complicated apparatus can be operated very reliably together with the 100 keV polarized source of MESA. Statistical errors in double scattering require run times of several days in order to achieve $\Delta S_{\mathrm{eff,stat.}}/S_{\mathrm{eff}} < 0.5\%$, whereas the operation of the polarimeter after its calibration will be in single scattering which allows measurements at the desired statistical accuracy level within minutes. The systematical errors are not yet under control at the desired level of accuracy and require more intense research in particular on the control of spurious asymmetries and backgrounds.

7. Summary and Conclusions

In this review, we have described the standard, common techniques used for measurements of electron beam polarimetry; Mott scattering, Møller scattering, and Compton scattering. Until recently, only moderate precision has been required by the experiments that make use of ∼GeV-level electron beams. However, recent and future parity violating electron scattering experiments have pushed precision requirements to <1%. Evolutionary developments in all three standard techniques have resulted in systematic uncertainties of 1% or slightly better, but further work is required to achieve the stringent requirements presented by future PVeS experiments, <0.5%.

Comparisons between multiple precision techniques will be crucial to verify the claimed precision of any particular device. In addition, new techniques are under development to supplement the existing standard measurements.

Acknowledgments

The authors are indebted to Timothy Gay for input on the AESOP Project and Matt Poelker and Mark Dalton for comments on early drafts of this review.

This work is supported by the United States Department of Energy's Office of Science, Contract Number DE-FG02-07ER41522 and Contract Number DE-AC05-06OR23177 under which Jefferson Science Associates, LCC operates the Thomas Jefferson National Accelerator Facility.

References

1. P. S. Cooper *et al.*, *Phys. Rev. Lett.* **34** (1975) 1589, doi:10.1103/PhysRevLett.34.1589.
2. M. J. Alguard *et al.*, *Phys. Rev. Lett.* **37** (1976) 1258, doi:10.1103/PhysRevLett.37.1258.
3. M. J. Alguard *et al.*, *Phys. Rev. Lett.* **37** (1976) 1261, doi:10.1103/PhysRevLett.37.1261.
4. V. Punjabi, C. F. Perdrisat, M. K. Jones, E. J. Brash and C. E. Carlson, *Eur. Phys. J. A* **51** (2015) 79, arXiv:1503.01452 [nucl-ex], doi:10.1140/epja/i2015-15079-x.
5. Jefferson Lab Hall A Collab. (M. K. Jones *et al.*), *Phys. Rev. Lett.* **84** (2000) 1398, arXiv:nucl-ex/9910005 [nucl-ex], doi:10.1103/PhysRevLett.84.1398.

6. C. A. Aidala, S. D. Bass, D. Hasch and G. K. Mallot, *Rev. Mod. Phys.* **85** (2013) 655, arXiv:1209.2803 [hep-ph], doi:10.1103/RevModPhys.85.655.
7. C. Y. Prescott *et al.*, *Phys. Lett. B* **77** (1978) 347, doi:10.1016/0370-2693(78)90722-0.
8. F. E. Maas and K. D. Paschke, *Prog. Part. Nucl. Phys.* **95** (2017) 209, doi:10.1016/j.ppnp.2016.11.001.
9. S. Abrahamyan *et al.*, *Phys. Rev. Lett.* **108** (2012) 112502, arXiv:1201.2568 [nucl-ex], doi:10.1103/PhysRevLett.108.112502.
10. SLAC E158 Collab. (P. L. Anthony *et al.*), *Phys. Rev. Lett.* **95** (2005) 081601, arXiv:hep-ex/0504049 [hep-ex], doi:10.1103/PhysRevLett.95.081601.
11. Qweak Collab. (T. Allison *et al.*), *Nucl. Instrum. Methods A* **781** (2015) 105, arXiv:1409.7100 [physics.ins-det], doi:10.1016/j.nima.2015.01.023.
12. PVDIS Collab. (D. Wang *et al.*), *Nature* **506** (2014) 67, doi:10.1038/nature12964.
13. E154 Collab. (K. Abe *et al.*), *Phys. Rev. Lett.* **79** (1997) 26, arXiv:hep-ex/9705012 [hep-ex], doi:10.1103/PhysRevLett.79.26.
14. HERMES Collab. (A. Airapetian *et al.*), *Phys. Rev. D* **75** (2007) 012007, arXiv:hep-ex/0609039 [hep-ex], doi:10.1103/PhysRevD.75.012007.
15. E. J. Beise, M. L. Pitt and D. T. Spayde, *Prog. Part. Nucl. Phys.* **54** (2005) 289, arXiv:nucl-ex/0412054 [nucl-ex], doi:10.1016/j.ppnp.2004.07.002.
16. A4 Collab. (F. E. Maas *et al.*), *Phys. Rev. Lett.* **93** (2004) 022002, arXiv:nucl-ex/0401019 [nucl-ex], doi:10.1103/PhysRevLett.93.022002.
17. SLD Collab. (K. Abe *et al.*), *Phys. Rev. Lett.* **86** (2001) 1162, arXiv:hep-ex/0010015 [hep-ex], doi:10.1103/PhysRevLett.86.1162.
18. N. Berger *et al.*, *J. Univ. Sci. Tech. China* **46** (2016) 481, arXiv:1511.03934 [physics.ins-det], doi:10.3969/j.issn.0253-2778.2016.06.006.
19. MOLLER Collab. (J. Benesch *et al.*), arXiv:1411.4088 [nucl-ex].
20. SoLID Collab. (J. P. Chen *et al.*), arXiv:1409.7741 [nucl-ex].
21. A. Accardi *et al.*, *Eur. Phys. J. A* **52** (2016) 268, arXiv:1212.1701 [nucl-ex], doi:10.1140/epja/i2016-16268-9.
22. N. F. Mott, *Proc. R. Soc. Lond. A*: *Math. Phys. Eng. Sci.* **124** (1929) 425, doi:10.1098/rspa.1929.0127.
23. S. Qiao and A. Kakizaki, *Rev. Sci. Instrum.* **68** (1997) 4017, doi:10.1063/1.1148381.
24. D. D. Neufeld, H. Aliabadi and F. B. Dunning, *Rev. Sci. Instrum.* **78** (2007) 025107, doi:10.1063/1.2536677.
25. V. N. Petrov, V. V. Grebenshikov, B. D. Grachev and A. S. Kamochkin, *Rev. Sci. Instrum.* **74** (2003) 1278, doi:10.1063/1.1535736.
26. J. McCarter, M. Stutzman, K. Trantham, T. Anderson, A. Cook and T. Gay, *Nucl. Instrum. Methods A* **618** (2010) 30, doi:10.1016/j.nima.2010.02.123.
27. J. Kessler, *Rev. Mod. Phys.* **41** (1969) 3, doi:10.1103/RevModPhys.41.3.
28. T. J. Gay and F. B. Dunning, *Rev. Sci. Instrum.* **63** (1992) 1635, doi:10.1063/1.1143371.
29. J. Kessler, *Polarized Electrons* (Springer, 1985).
30. J. W. Motz, H. Olsen and H. W. Koch, *Rev. Mod. Phys.* **36** (1964) 881, doi:10.1103/RevModPhys.36.88.
31. N. Sherman, *Phys. Rev.* **103** (1956) 1601, doi:10.1103/PhysRev.103.1601.
32. P. Ugin̆cius, H. Überall and G. Rawitscher, *Nucl. Phys. A* **158** (1970) 418, doi:10.1016/0375-9474(70)90193-4.
33. X. Roca-Maza, M. Centelles, F. Salvat and X. Viñas, *Phys. Rev. C* **78** (2008) 044332, doi:10.1103/PhysRevC.78.044332.
34. J. Sromicki *et al.*, *Phys. Rev. Lett.* **82** (1999) 57, doi:10.1103/PhysRevLett.82.57.

35. S.-R. Lin, N. Sherman and J. K. Percus, *Nucl. Phys.* **45** (1963) 492, doi:10.1016/0029-5582(63)90824-1.
36. X. Roca-Maza, arXiv:1710.08683 [physics.atom-ph].
37. V. M. Shabaev, V. A. Yerokhin, T. Beier and J. Eichler, *Phys. Rev. A* **61** (2000) 052112, doi:10.1103/PhysRevA.61.052112.
38. W. Johnson, C. Carroll and C. Mullin, *Phys. Rev.* **126** (1962) 352, doi:10.1103/PhysRev.126.352.
39. V. Tioukine, K. Aulenbacher and E. Riehn, *Rev. Sci. Instrum.* **82** (2011) 033303, doi:10.1063/1.3556593.
40. M. Steigerwald, *AIP Conf. Proc.* **570** (2001) 935, doi:10.1063/1.1384229.
41. K. Aulenbacher and V. Tioukine, *Ab initio* calculations of effective Sherman functions in MeV Mott scattering, in 18*th Int. Spin Physics Symp.*, Charlottesville, Virginia, October 6–11, 2008, eds. D. Crabb, D. Day, S. Liuti, X. Zheng, M. Poelker and Y. Prok, AIP Conference Proceedings, Vol. 1149 (Springer, Berlin, 2008), pp. 1155–1159.
42. M. A. Khakoo, D. Roundy, C. Hicks, N. Margolis, E. Yeung, A. W. Ross and T. J. Gay, *Phys. Rev. A* **64** (2001) 052713, doi:10.1103/PhysRevA.64.052713.
43. M. Steigerwald, MeV Mott polarimetry at Jefferson lab, in 14*th Int. Spin Physics Symp.*, Osaka, Japan, October 16–21, 2000, eds. K. Hatanaka, H. Ejiri, K. Imai and T. Nakano, AIP Conference Proceedings, Vol. 570 (Springer, New York, 2001), p. 935.
44. M. Dehn, K. Aulenbacher, R. Heine, H. J. Kreidel, U. Ludwig-Mertin and A. Jankowiak, *Eur. Phys. J. ST* **198** (2011) 19, doi:10.1140/epjst/e2011-01481-4.
45. H. Frauenfelder *et al.*, *Phys. Rev.* **107** (1957) 643.
46. C. Møller, *Ann. Phys.* **406** (1932) 531, doi:10.1002/andp.19324060506.
47. A. A. Kresnin and L. N. Rosentsveig, *Sov. JETP* **5** (1957) 288, http://www.jetp.ac.ru/cgi-bin/e/index/e/5/2/p288?a=list.
48. A. M. Bincer, *Phys. Rev.* **107** (1957) 1434, doi:10.1103/PhysRev.107.1434.
49. N. M. Shumeiko and J. G. Suarez, *J. Phys. G* **26** (2000) 113, arXiv:hep-ph/9912228 [hep-ph], doi:10.1088/0954-3899/26/2/302.
50. A. Ilyichev and V. Zykunov, *Phys. Rev. D* **72** (2005) 033018, arXiv:hep-ph/0504191 [hep-ph], doi:/10.1103/PhysRevD.72.033018.
51. G. G. Scott, *Rev. Mod. Phys.* **34** (1962) 102, doi:10.1103/RevModPhys.34.102.
52. C. D. Graham, Jr., *J. Appl. Phys.* **53** (1982) 2032, doi:10.1063/1.330695.
53. G. G. Scott and H. W. Sturner, *Phys. Rev.* **184** (1969) 490, doi:10.1103/PhysRev.184.490.
54. R. Pauthenet, *J. Appl. Phys.* **53** (1982) 2029, doi:10.1063/1.330694.
55. L. G. Levchuk, *Nucl. Instrum. Methods A* **345** (1994) 496, doi:10.1016/0168-9002(94)90505-3.
56. M. Swartz *et al.*, *Nucl. Instrum. Methods A* **363** (1995) 526, arXiv:hep-ex/9412006 [hep-ex], doi:10.1016/0168-9002(95)00384-3.
57. B. Wagner, H. G. Andresen, K. H. Steffens, W. Hartmann, W. Heil and E. Reichert, *Nucl. Instrum. Methods A* **294** (1990) 541, doi:10.1016/0168-9002(90)90296-I.
58. J. Arrington, E. J. Beise, B. W. Filippone, T. G. O'Neill, W. R. Dodge, G. W. Dodson, K. A. Dow and J. D. Zumbro, *Nucl. Instrum. Methods A* **311** (1992) 39, doi:10.1016/0168-9002(92)90849-Y.
59. K. B. Beard *et al.*, *Nucl. Instrum. Methods A* **361** (1995) 46, doi:10.1016/0168-9002(95)00144-1.
60. H. R. Band, G. Mitchell, R. Prepost and T. Wright, *Nucl. Instrum. Methods A* **400** (1997) 24, doi:10.1016/S0168-9002(97)00984-4.

61. P. Steiner, A. Feltham, I. Sick, M. Zeier and B. Zihlmann, *Nucl. Instrum. Methods A* **419** (1998) 105, doi:10.1016/S0168-9002(98)00938-3.
62. A. V. Glamazdin *et al.*, *Fizika B* **8** (1999) 91, arXiv:hep-ex/9912063 [hep-ex].
63. T. Bahlo, J. Enders, T. Kürzeder, N. Pietralla and J. Wissmann, Design of a very compact 130 MeV Møller polarimeter for the S-Dalinac, in *5th Int. Beam Instrumentation Conf.* (*IBIC '16*), Barcelona, Spain, September 13–18, 2016 (2017), pp. 438–440.
64. L. V. De bever, J. Jourdan, M. Loppacher, S. Robinson, I. Sick and J. Zhao, *Nucl. Instrum. Methods A* **400** (1997) 379, doi:10.1016/S0168-9002(97)00961-3.
65. M. Hauger *et al.*, *Nucl. Instrum. Methods A* **462** (2001) 382, arXiv:nucl-ex/9910013 [nucl-ex], doi:10.1016/S0168-9002(01)00197-8.
66. C. Y. Prescott *et al.*, *Phys. Lett. B* **84** (1979) 524, doi:10.1016/0370-2693(79)91253-X.
67. M. Meyerhoff *et al.*, *Phys. Lett. B* **327** (1994) 201, doi:10.1016/0370-2693(94)90718-8.
68. P. Bartsch, Aufbau eines Møller-Polarimeters für die Drei-Spektrometer-Anlage und Messung der Helizitätsasymmetrie in der Reaktion $p(\vec{e}, e'p)\pi^0$ im Bereich der Δ-Resonanz, Ph.D. thesis, Institut für Kernphysik, Mainz University (2001).
69. T. Speckner, G. Anton, W. von Drachenfels, F. Frommberger, K. Helbing, M. Hoffmann, B. Kiel, T. Michel, J. Naumann and G. Zeitler, *Nucl. Instrum. Methods A* **519** (2004) 518, doi:10.1016/j.nima.2003.11.016.
70. O. Glamazdin, *Nuovo Cimento C* **35** (2012) 176, doi:10.1393/ncc/i2012-11275-8.
71. CLAS Collab. (B. A. Mecking *et al.*), *Nucl. Instrum. Methods A* **503** (2003) 513, doi:/10.1016/S0168-9002(03)01001-5.
72. J. Magee, *PoS* **PSTP2013** (2013) 039.
73. F. Lipps and H. Tolhoek, *Physica* **20** (1954) 85, doi:10.1016/S0031-8914(54)80018-8.
74. F. R. Arutyunian and V. A. Tumanian, *Phys. Lett.* **4** (1963) 176, doi:10.1016/0031-9163(63)90351-2.
75. R. H. Milburn, *Phys. Rev. Lett.* **10** (1963) 75, doi:10.1103/PhysRevLett.10.75.
76. M. L. Swartz, *Conf. Proc.* **C8708101** (1987) 83.
77. C. Y. Prescott, SLAC-TN-73-001 (1973).
78. C. K. Sinclair, J. J. Murray, P. R. Klein and M. Rabin, *IEEE Trans. Nucl. Sci.* **16** (1969) 1065, doi:10.1109/TNS.1969.4325441.
79. B. Norum and T. P. Welch, CEBAF LOI 93-012 (1993).
80. S. Escoffier *et al.*, *Nucl. Instrum. Methods A* **551** (2005) 563, arXiv:physics/0504195 [physics], doi:10.1016/j.nima.2005.05.067.
81. M. Baylac *et al.*, *Phys. Lett. B* **539** (2002) 8, arXiv:hep-ex/0203012 [hep-ex], doi:10.1016/S0370-2693(02)02091-9.
82. A. Narayan *et al.*, *Phys. Rev. X* **6** (2016) 011013, arXiv:1509.06642 [nucl-ex], doi:10.1103/PhysRevX.6.011013.
83. S. Baudrand *et al.*, *J. Instrum.* **5** (2010) P06005, arXiv:1005.2741 [physics.ins-det], doi:10.1088/1748-0221/5/06/P06005.
84. A4 Collab. (Y. Imai), *Prog. Part. Nucl. Phys.* **55** (2005) 332, doi:10.1016/j.ppnp.2005.01.003.
85. M. Beckmann *et al.*, *Nucl. Instrum. Methods A* **479** (2002) 334, arXiv:physics/0009047 [physics.ins-det], doi:10.1016/S0168-9002(01)00901-9.
86. SLD Collab. (M. Woods), The scanning Compton polarimeter for the SLD experiment, in *Proc. 12th Int. Symp. High-Energy Spin Physics*, *SPIN* 96, Amsterdam, Netherlands, September 10–14, 1996 (1996), pp. 843–845, arXiv:hep-ex/9611005 [hep-ex].

87. A. A. Sokolov and I. M. Ternov, *Sov. Phys. Dokl.* **8** (1964) 1203.
88. D. Gustavson, J. J. Murray, T. J. Phillips, R. Schwitters, C. K. Sinclair, J. R. Johnson, R. Prepost and D. E. Wiser, *Nucl. Instrum. Methods* **165** (1979) 177, doi:10.1016/0029-554X(79)90268-4.
89. Crystal Ball, ARGUS Collab. (D. P. Barber *et al.*), *Phys. Lett. B* **135** (1984) 498, doi:10.1016/0370-2693(84)90323-X.
90. A. S. Artamonov *et al.*, *Phys. Lett. B* **118** (1982) 225, doi:10.1016/0370-2693(82)90633-5.
91. CUSB Collab. (W. W. MacKay *et al.*), *Phys. Rev. D* **29** (1984) 2483, doi:10.1103/PhysRevD.29.2483.
92. D. P. Barber *et al.*, *Nucl. Instrum. Methods A* **338** (1994) 166, doi:10.1016/0168-9002(94)91311-0.
93. R. Koop, W. Hillert and M. Switka, Compton polarimetry at ELSA — Beamline and detector optimization, in *Proc. 7th Int. Particle Accelerator Conference* (*IPAC* 2016), Busan, Korea, May 8–13, 2016 (2016), p. MOPMB010.
94. I. Passchier, C. W. de Jager, N. H. Papadakis, N. P. Vodinas, D. W. Higinbotham and B. E. Norum, *Nucl. Instrum. Methods A* **414** (1998) 446, arXiv:physics/9902011 [physics], doi:10.1016/S0168-9002(98)00630-5.
95. W. A. Franklin, T. Akdogan, D. Dutta, M. Farkhondeh, M. Hurwitz, J. L. Matthews, E. Tsentalovich, W. Turchinetz, T. Zwart and E. C. Booth, *AIP Conf. Proc.* **675** (2003) 1058, doi:10.1063/1.1607296.
96. BLAST Collab. (W. A. Franklin), The MIT-Bates Compton polarimeter for the South Hall Ring, in *Proc. 16th Int. Spin Physics Symp. and Workshop on Polarized Electron Sources and Polarimeters*, Trieste, Italy, October 10–16, 2004 (2004), pp. 714–717.
97. J. Diefenbach, Y. Imai, J. H. Lee, F. Maas and S. Taylor, *Eur. Phys. J. A* **32** (2007) 555, doi:10.1007/978-3-540-74413-9_46, 10.1140/epja/i2006-10443-7.
98. J. H. Lee, Concept and realization of the A4 Compton backscattering polarimeter at MAMI, Ph.D. thesis Institut für Kernphysik, Mainz University (2008).
99. M. Placidi and R. Rossmanith, *Nucl. Instrum. Methods A* **274** (1989) 79, doi:10.1016/0168-9002(89)90367-7.
100. R. Assmann, Polarization in LEP, in *Proc. 4th LEP Performance Workshop*, Chamonix, France, January 4th 17–21, 1994 (1994), pp. 353–364.
101. POL2000 Collab. (B. Sobloher), Polarisation and polarimetry at HERA, in *Proc. 13th Int. Workshop on Polarized Sources and Targets & Polarimetry* (*PSTP* 2009), Ferrara, Italy, September 7–11, 2009 (2011), pp. 78–89, doi:10.1142/9789814324922_0010.
102. HAPPEX Collab. (A. Acha *et al.*), *Phys. Rev. Lett.* **98** (2007) 032301, arXiv:nucl-ex/0609002 [nucl-ex], doi:10.1103/PhysRevLett.98.032301.
103. M. Friend *et al.*, *Nucl. Instrum. Methods A* **676** (2012) 96, arXiv:1108.3116 [physics.ins-det], doi:10.1016/j.nima.2012.02.041.
104. A. Rakhman *et al.*, *Nucl. Instrum. Methods A* **822** (2016) 82, arXiv:1601.00251 [physics.ins-det], doi:10.1016/j.nima.2016.03.085.
105. J. C. Cornejo, Compton scattering polarimetry for the determination of the proton's weak charge through measurements of the parity-violating asymmetry of $^1\mathrm{H}(e,e')\mathrm{p}$, Ph.D. thesis, College of William and Mary (2016).
106. SLD Collab. (K. Abe *et al.*), *Phys. Rev. Lett.* **84** (2000) 5945, arXiv:hep-ex/0004026 [hep-ex], doi:10.1103/PhysRevLett.84.5945.
107. M. Friend, G. B. Franklin and B. Quinn, *Nucl. Instrum. Methods A* **676** (2012) 66, arXiv:1108.3096 [physics.ins-det], doi:10.1016/j.nima.2012.02.015.

108. Under a Creative Commons License, https://creativecommons.org/licenses/by/3.0/.
109. V. Brisson, R. Chiche, M. Jacquet, C. Pascaud, V. Soskov, Z. Zhang, F. Zomer, M. Beckingham and N. Coppola, *J. Instrum.* **5** (2010) P06006, arXiv:1005.2742 [physics.ins-det], doi:10.1088/1748-0221/5/06/P06006.
110. N. Vansteenkiste, P. Vignolo and A. Aspect, *J. Opt. Soc. Am. A* **10** (1993) 2240, doi:10.1364/JOSAA.10.002240.
111. M. Woods, SLD Compton polarimeter, Jefferson Lab Workshop on Precision Electron Beam Polarimetry, Joint University of Connecticut, Hampton University (2003), https://www.jlab.org/polarimetry/talks/woods_sld.pdf.
112. J. M. Grames *et al.*, *Phys. Rev. ST Accel. Beams* **7** (2004) 042802, Erratum **13** (2010) 069901, doi:10.1103/PhysRevSTAB.7.042802, 10.1103/PhysRevSTAB.13.069901.
113. Qweak Collab. (D. Androic *et al.*), *Phys. Rev. Lett.* **111** (2013) 141803, arXiv:1307.5275 [nucl-ex], doi:10.1103/PhysRevLett.111.141803.
114. J. A. Magee *et al.*, *Phys. Lett. B* **766** (2017) 339, arXiv:1610.06083 [physics.ins-det], doi:10.1016/j.physletb.2017.01.026.
115. Under a Creative Commons License, http://creativecommons.org/licenses/by/4.0/.
116. E. Chudakov and V. Luppov, *IEEE Trans. Nucl. Sci.* **51** (2004) 1533.
117. E. Chudakov and V. Luppov, *Eur. Phys. J.* **24** (2005) 123, doi:10.1140/epjad/s2005-04-028-8.
118. E. Chudakov, *Nuovo Cimento C* **35** (2012) 181, doi:10.1393/ncc/i2012-11268-7.
119. N. B. Clayburn and T. J. Gay, *Phys. Rev. Lett.* **119** (2017) 093401, doi:10.1103/PhysRevLett.119.093401.
120. B. G. Birdsey, H. M. Al-Khateeb, M. E. Johnston, T. C. Bowen, T. J. Gay, V. Zeman and K. Bartschat, *Phys. Rev. A* **60** (1999) 1046, doi:10.1103/PhysRevA.60.1046.
121. T. J. Gay, J. E. Furst, K. W. Trantham and W. M. K. P. Wijayaratna, *Phys. Rev. A* **53** (1996) 1623, doi:10.1103/PhysRevA.53.1623.
122. B. Collin, J. Arianer, S. Essabaa, R. Frascaria, R. Gacougnolle, R. Kunne, K. Aulenbacher and V. Tioukine, *Nucl. Instrum. Methods A* **534** (2004) 361, doi:10.1016/j.nima.2004.06.180.
123. K. Aulenbacher, P. A. Bartolomé, M. Molitor and V. Tioukine, *AIP Conf. Proc.* **1563** (2013) 247, doi:10.1063/1.4829421.
124. T. J. Gay, *J. Phys. B*: *At. Mol. Phys.* **16** (1983) L553, doi:10.1088/0022-3700/16/18/005.
125. M. Pirbhai, D. M. Ryan, G. Richards and T. J. Gay, *Rev. Sci. Instrum.* **84** (2013) 053113, doi:10.1063/1.4807745.
126. A. Gellrich, K. Jost and J. Kessler, *Rev. Sci. Instrum.* **61** (1990) 3399, doi:10.1063/1.1141591.
127. A. Gellrich and J. Kessler, *Phys. Rev. A* **43** (1991) 204, doi:10.1103/PhysRevA.43.204.
128. S. Mayer, T. Fischer, W. Blaschke and J. Kessler, *Rev. Sci. Instrum.* **64** (1993) 952, doi:10.1063/1.1144148.
129. H. Hopster and D. L. Abraham, *Rev. Sci. Instrum.* **59** (1988) 49, doi:10.1063/1.1139964.
130. K. Aulenbacher, I. Alexander and V. Tioukine, *Nuovo Cimento* **C035N04** (2012) 186, doi:10.1393/ncc/i2012-11301-y.